First Progress Report

DIVISION OF PHYSICAL RESEARCH
ENERGY RESEARCH AND DEVELOPMENT ADMINISTRATION
Washington, D.C. 20545

for

STUDIES OF FUNDAMENTAL FACTORS CONTROLLING CATALYZATION OF REACTIONS OF GASES WITH CARBONACEOUS SOLIDS

April 1977

RESEARCH LABORATORY
UNITED STATES STEEL CORPORATION
MONROEVILLE PENNSYLVANIA

Progress Report

Submitted to

Division of Physical Research
ERDA
Washington, D.C. 20545

Studies of Fundamental Factors Controlling Catalyzation of Reactions of Gases With Carbonaceous Solids

R. M. Fisher, C. G. Shirley, A. Szirmae
J. V. Mahoney, F. C. Schwerer

Abstract

Flakes of natural graphite exposed to various H_2-H_2O-He atmospheres at temperatures from 650° to 1100°C after deposition of small particles of iron have been examined in the SEM and MVEM. The characteristics of surface channels resulting from iron-catalyzed reactions producing CO and/or CH_4 appear to depend on temperature and to a lesser extent on P_{H_2O} level. Very narrow, parallel-sided channels catalyzed by small iron particles, initiated at ledge steps on the cleaved graphite, take on <11$\bar{2}$0> directions at low temperatures and in moist atmospheres, whereas at high temperatures broad wavy tracks result from movement of large particles. Very broad reaction zones are wetted by an unknown iron-silicon phase forming thin ribbons of what appear to be single crystals on samples heated in dry H_2 at 1100°C. Simple models of iron-catalyzed channeling reactions have been examined on the basis of heat balance, gas diffusion, surface migration and other considerations to define limiting conditions and suggest new experimental observations.

Research Laboratory
U. S. Steel Corporation
Monroeville, Pa. 15146

April 1977

Table of Contents

Summary

Considerable effort has gone into assembly of experimental apparatus and development of sample-preparation techniques and methods for examining specimens in the scanning electron microscope (SEM) and million volt electron microscope (MVEM). Some 60 different samples have been reacted and examined, an extensive bibliography has been collected and perused, and simple theoretical models have been considered as guides to interpretation and further experimentation.

Flakes of natural (Ticonderoga) graphite have been exposed to H_2-H_2O-He atmospheres over the range $P_{H_2O} = \sim 10^{-5}$ to 5×10^{2}, $P_{H_2O} = 0$ to ~ 1, and $P_{He} = 0$ to ~ 1 atmospheres at temperatures from 650° to 1200°C. Flow rates of high-purity tank gases are measured and the O_2 activity is continuously monitored with a solid-state sensor. The recorded values are entered through a remote terminal to compute and print out P_{H_2O} and P_{O_2} on each run for data-logging purposes.

Calculations for thermodynamic equilibrium for several combinations of possible gas-phase and gas-solid reactions have been obtained as guides in experimental design and interpretation.

Small spherical particles of Fe (d = 100 to 5000 Å) are formed on the surface of the graphite flakes in two steps: (1) vacuum deposition of Fe masses equivalent to a 25 to 1000 Å thick continuous film, and (2) subsequent annealing of the sample in dry hydrogen at 750°C.

SEM and MVEM observations of the surface channels resulting from the Fe-catalyzed reaction producing CO and/or CH_4 have revealed variations in their nature which appear to be dependent on temperature and to a lesser extent on P_{H_2O} level. Very narrow, parallel-sided channels catalyzed by small iron particles initiated at ledge steps on the cleaved graphite take on <11$\bar{2}$0> directions at low temperatures and moist ($P_{H_2O} = 10^{-3}$ to 10^{-2}) atmospheres, whereas at high temperatures broad wavy tracks are left by large iron particles, which often continue to grow by the addition of other iron particles encountered in their path.

At 1100°C in very dry hydrogen, the edges of the very broad reaction zones are wetted by an iron phase forming thin ribbons of what appear to be single crystals. The electron diffraction patterns of these particles have not been identified. Spectrochemical analysis in the SEM and EPMA has revealed the presence of a large amount of silicon in the particles, which may originate from impurities in the graphite or possibly from the quartz furnace tube. Measurements of the length of the longest channels on selected specimens show a variation of not more than a factor of 20 over the full temperature range in keeping with a low (∿10 kcal) activation energy. Simple models for Fe-catalyzed cahnneling reactions have been examined on the basis of heat balance, gas diffusion, surface migration and other considerations to define limiting conditions and to suggest new experimental observations.

Preliminary gas analysis has verified that methane is the primary reaction product in dry hydrogen at 1000°C. Future efforts will be concentrated on determining the source of silicon found in the iron particles and identifying the silicon-iron phase, obtaining more quantitative data on channeling rates and orientations as a function of temperature and atmosphere, correlating the concentration of CH_4 and CO produced with track morphology, and attempting to establish the state of the iron during the channeling reaction (i.e., alpha, gamma, or liquid).

Introduction

This report is a summary of progress since this project was initiated June 1, 1976. It includes a brief statement of the rationale and basic orientation of the program, a description of the experimental procedure established, a summary of the results to date, an outline of some theoretical ideas for interpreting the observations and suggesting further measurements, plans for future research and an extensive bibliography relevant to the program. It is anticipated that completion of additional experimental observations and further refinement of their interpretation as discussed in this progress report will permit preparation of a detailed report of the research results suitable for publication to serve as the first year final report.

Research Rationale

In recent years it has become quite apparent that increased utilization of the vast U. S. coal resources is the most reasonable and immediate solution to the problems associated with the continued U. S. dependence on petroleum energy and natural gas. Until recently the relatively high costs of mining, processing and transporting coal have inhibited the development of coal technology, so that most modern technological processes depend on gaseous and liquid fuels. Therefore, an important element in making coal-derived energy readily useful to modern technology is the conversion of coal to gaseous or liquid fuels. Potent catalysts are essential

to efficient conversion processes, but it is difficult and time consuming to identify suitable catalytical material on a purely empirical basis. Hence, the importance of fundamental studies of catalyzed carbon-gas reactions.

There have been many studies of both catalyzed and uncatalyzed carbon-gas reactions. Most quantitative studies have been carried out on bulk samples of carbons ranging from graphite to coal, and the results have been extremely useful to the technology of coal utilization. There have also been a number of more qualitative microscopic observations of reaction morphology. Although a good deal of light has been shed on the fundamental reaction processes by these studies, there is still much controversy and little more than qualitative agreement between the results of various workers in the field. Possible reasons for this are (1) a complete morphological characterization of a bulk sample is very difficult if not impossible because parameters such as porosity, particle size, impurity levels, etc. are hard to control and may even change in the course of a reaction; (2) experiments often cover different temperature and partial-pressure ranges and mechanisms may actually be different in different regimes; (3) even if the mechanism does not change, data are often summarized by fitting to a Langmuir-type expression which fits the limited regime, but an expression more complicated (and yet consistent with a single mechanism) may be necessary to fit the larger regime encompassing all experiments.

The central idea of the present project is to carry out a quantitative microscopic kinetic study on a very well characterized carbon (single-crystal graphite) in order to eliminate many of the morphological parameters which obscure the fundamental reaction processes. This is possible because one crystallographically well-defined feature (a step, pit, reaction channel) can be studied. The data obtained from such an experiment should be far more reproducible than bulk measurements and be amenable to more precise modelling. We have chosen to confine our attention initially to catalyzed oxidation, namely the iron-catalyzed graphite-water vapor reaction, and to catalyzed hydrogenation in dry hydrogen and to study these in detail with a continuous range of partial pressures, rather than to attempt a broad survey of many catalysts and reactions.

Experimental Methods

Observations of the catalytic effect of iron on C/H_2O C/H_2 reactions are being carried out on small single-crystal flakes of naturally occurring graphite from the Ticonderoga region of New York. The procedure used so far has been to evaporate pure iron onto the flakes in a vacuum and then to reduce the iron and react the samples in a furnace-gas-handling system which gives good control of the partial pressures of water and hydrogen. The samples are then examined in the USS high-voltage electron microscope (HVEM) or an ETEC scanning electron microscope (SEM) to observe the iron particles and their activity on the graphite surface. The

largest part of the experimental effort so far has been devoted to the development of a furnace-gas-handling system suitable for our purposes, and to a qualitative survey of the results obtained by varying the various parameters under our control over the ranges permitted by our equipment. In further work, more precise measurements of particle sizes, channel dimensions etc. over narrower but interesting ranges will be made using the computer-based stereoscope in our laboratory.

The central component of the gas-handling equipment is an oxygen sensor which continuously monitors the oxygen potential of the exhaust gases, as shown in Figures 1 and 2. The rate of carbon gasification is negligible when compared with the flow rates used (about 1000 ml/min) so the inlet and exhaust gases have negligibly different compositions (and oxygen potentials). The gas mixture composition can be set by using the oxygen potential. For example, a wet H_2/He mixture can be generated by noting the oxygen potential of purified (dry) hydrogen, then reducing the potential a specified amount by dilution with helium, and then reducing the potential by another specified amount by wetting the gas in the saturator. The system can heat samples at temperatures to 1200°C in atmospheres with P_{H_2O} ranging from 6×10^{-6} atm to 0.5 atm and with any value of P_{H_2}/P_{He}. All procedures including the gas-mixing procedure have been optimized and standardized to maximize efficiency and reproducibility. See Appendix I for a summary of the procedures. A

computer program has been written to streamline calculations of the gas-mixing procedure. See Appendix II for lists of the computer programs.

The furnace has been set on wheels to obtain fast heating and cooling rates so that the reaction temperature and time are fairly well defined. The sample temperature rises from room temperature to 1000°C in one minute. Rapid adjustments of sample temperature can be achieved by moving the sample to different zones in the furnace. An initial degassing of the quartz sample tube is also facilitated by this arrangement. Flakes of graphite are placed in a quartz boat in the cold part of the furnace tube with a ball bearing next to the boat and the furnace is rolled onto the quartz tube so that the end reaches a temperature higher than the ultimate reaction temperature. After holding this arrangement for several minutes (to degas the interior quartz tube wall) the furnace is rolled away from the tube and the tube is allowed to cool. The sample boat is then pushed into the end of the tube (without opening the tube to air) by using a magnet to roll the ball bearing behind the boat. The system is ready to begin a run at this stage.

A run usually begins with an initial reduction stage to ensure that the as-evaporated iron is indeed metallic. It is important, however, to ensure that this stage causes no appreciable reaction on the surface of the graphite flake. The temperature and oxygen potential profiles of a run are recorded on a two-pen chart

recorder along with all the other details of the run. The gas compositions and flow rates at the sample are computed and summarized by the program "GASCOMP3". The reacted flakes are then examined in the SEM or the HVEM.

Gas samples can be taken downstream from the reaction zone for analysis of CO and CH_4 content by chromatography. Chemical analysis of a bulk sample of the graphite used for the studies indicated the presence of substantial amounts of silicon (4.7%), aluminum (1.5%), and calcium (0.76%). However, these elements presumably are associated with mineral inclusions and do not accurately reflect the composition of freshly cleaved surfaces.

Electron Microscope Observations

Scanning electron micrographs of a typical graphite flake as used for reaction channeling experiments are shown in Figure 3. A representative region containing a large number of twins is shown at higher magnification. The occurrence of twins is useful for the experiments because the twin traces provide an orientation for any region on the surface for comparison with the directions of reaction channels. The surface of the cleaved graphite is generally quite smooth; occasionally fine particles of silicate inclusions or other impurities are present.

Freshly cleaved surfaces are coated with iron by vacuum evaporation. Nominal film thicknesses ranging from 40 Å to 1000 Å have been used for the various experiments. After vacuum evaporation

the sample of graphite is heat-treated in a dry hydrogen atmosphere to agglomerate the film into small essentially spherical particles. Examples of the various stages of the formation of fine particles of metallic iron are illustrated in Figure 4. The first stage is the breakup of the film at the edges into small particles, and this continues until the film is essentially gone. Surface ledges are decorated, as illustrated in Figure 4C, by small particles of iron which form along the steps on the surface. Sometimes large particles form as a result of surface migration and grow in size as they sweep over the surface and accumulate iron. An example of this phenomenon is shown in Figure 4D. A very small amount of reaction occurs during the annealing process, particularly if the time is prolonged. A nominal treatment time of 20 minutes results in very little catalytic attack. A summary of reacted samples examined in detail is listed in Table I according to reaction temperature and atmosphere.

A typical example of channeling attack in moist hydrogen at 800°C catalyzed by the presence of iron particles is shown in Figure 5. It may be noted that the channels originate at the ledge steps on the graphite surface and progress inward from there. Attack at sites away from the ledges is extremely rare and presumably even then is associated with some inhomogeneity at the graphite surface. Under these conditions the channels tend to run parallel to $\langle 11\bar{2}0 \rangle$ directions on the graphite surface.

The reacted surface has a quite different appearance if the particles are extremely large. In Figure 6 an example is shown of a 1000 Å layer of iron that had been deposited and then reacted for 1-1/2 hours at 700°C. In this case the large particles are immobile but evidence of attack around the particle may be seen. This may be associated with the extremely small particles of iron which may be noted around the edge of the reacted region. This type of reaction is discussed later in this report.

The appearance of the channel changes quite markedly with reaction temperature and also with the water content of the atmosphere. Examples of the different types are shown in Figure 7. Figure 7A shows narrow, straight channels which obviously initiated at the ledges on the graphite surface in a sample reacted in moderately wet hydrogen at 800°C. At 1000°C, the particles grow larger and the reaction trail left behind the iron particle moving over the surface is generally wavy, although comprising short segments of straight, parallel-side channels.

At 1100°C the appearance of the reaction zone is again quite different as the reactive channels tend to be very broad and the iron particles have a molten appearance. It is also clear that they tend to wet the edges of the channel. The three micrographs in Figure 7 illustrate the different channel types which tend to be associated with a particular temperature. However in most cases the reacted surfaces exhibit several types; that is, the straight channel

and wavy channels tend to occur together at low temperatures, and the wavy channels and the very broad terrace type tend to occur at the upper end of the temperature range explored.

The channels can also be seen by transmission electron microscopy in the million volt electron microscope. The resolution is higher in the transmission microscope so the details can be seen more clearly, but all areas of the graphite flake are not transparent so the observations are restricted to the edges of the graphite flakes. The example shown in Figure 8 also illustrates the difference in appearance of the particles when a hydrogen-helium atmosphere is used. In this case the particles remain as thin single crystals rather than the roughly spherical particles that occur at this temperature in a slightly moist hydrogen atmosphere. The strict crystallographic character of the channels is quite apparent; it may also be noted that when a particle becomes isolated from the sides of the reaction zone, the reaction stops.

Another example of reaction structure is shown in Figure 9. In this case relatively large particles were formed by depositing 1000 Å of iron, which resulted in micron-size particles after annealing. In this case the particles again show the smooth structure suggestive of melting and wet edges of the reaction zone on the graphite surface. In some cases a continuous film has formed along the edge step.

High voltage transmission micrographs of channels formed at 1100°C in atmosphere of 4×10^{-4} partial pressure of water vapor are shown in Figure 10. Both broad terrace reaction zones and narrow channels are evident for these experimental conditions.

Above 1000°C oxidation in wet hydrogen generates evidence of some uncatalyzed attack such as that shown in Figure 11. In this case the edges of the reaction channels and the terraces on the graphite take on a rough appearance; presumably this is the result of uncatalyzed direct attack by water vapor.

After reaction in very dry hydrogen at 1100°C, a different type of reaction zone was noted. Examples of three different cases are shown in Figure 12. In general, the channels tend to be very wide and the particles spread out and wet the edges of the reaction zone and actually in many cases leave a thin crystal film behind during the course of the reaction. A good example of this film may be noted in Figure 12B. The composition of these particles was checked by using the x-ray analysis facility on the scanning electron microscope, and a surprising amount of silicon was found to be associated with the particles as illustrated in Figure 13. The beam was stopped on a selected particle and the spectra shown in Figure 13B was obtained. X-ray images with characteristic iron and silicon radiation are shown in Figures 13C and D. These images demonstrate that a very large amount of silicon, possibly as much as 30 percent, is present in the particles.

The presence of silicon in the iron particles was also noted at 900°C, as shown in Figure 14. The concentration of silicon in general tends to be much less than at 1100°C, but occasional particles show more than the amount illustrated in this figure. The source of the silicon is uncertain at the present time. Calculations show that the partial pressure of SiO at 1100°C in dry hydrogen is of the order of 10^{-4}, so that hydrogen reduction of the quartz furnace tube could form a significant quantity of SiO which could deposit on the surface and react with the iron. The other possibility is that the silicon is present as an impurity in the graphite and accumulates in the iron as the reaction goes on. Bulk chemical analysis has shown the presence of a significant amount of silicon as well as calcium and other elements in the graphite. However, if mineral inclusions are the source of the silicon, contamination of the iron particles would not depend on reaction temperature and gas composition, as seems to be the case. More work is required to determine the origin of the silicon and its influence on the nature of reaction channelling.

In attempt to increase the contrast of the reaction channels for high voltage microscopy, a thin 50 Å film of gold was deposited on the surface after reaction had taken place. This vacuum deposition does enhance channel contrast considerably, as may be seen in the micrograph in Figure 15, and will be used extensively in further studies of reaction details.

A few experiments were conducted to react electrode-purity graphite planchets in the wet and dry hydrogen atmospheres used for studies on the graphite flakes. The planchets are much larger than the graphite flakes and reaction gases are produced in much larger quantites than with the very tiny (millimeter-size) flakes of graphite.

An example of the surface after reaction is shown in Figure 16. Figure 16A shows the interface between the region coated with 1000 Å of iron by vacuum evaporation and the uncoated surface. It may be noted that very little reaction occurs in the regions that are not coated with iron. The iron-rich region is seen to wet the surface of the graphite pits in some instances, and other iron particles remain as essentially spherical balls of iron promoting very rapid gasification of the planchets in dry hydrogen.

The gas reaction products were sampled and analyzed by chromotography and found to contain about 12 ppm methane and essentially no carbon monoxide. These experiments will be followed up more extensively in the future. The main point to note here is that marked catalytic acceleration of hydrogenation occurs on both single-crystal surfaces of graphite and polycrystalline planchets.

Summary of Experimental Observations

The main features of iron-catalyzed gasification of graphite may be summarized as follows:

1. Reaction tracks originate at edge steps and ledges on freshly cleaved surfaces of graphite.

2. Several different types of channels or tracks result from gasification reactions; these are illustrated schematically in Figure 17. One type is long, very narrow, straight channels with edges parallel to $\langle 11\bar{2}0 \rangle$ directions; these channels are characteristic of cases where iron particles are extremely small. In another type the particles are large, roughly spherical, and overhang the edges of the reaction channel as shown in Figure 17B. In this case the tracks tend to wander in direction and width and the edges are not necessarily parallel, although both take up the same crystallographic directions. The third type is shown in Figure 17C; here the iron spreads out into a very narrow ribbon along the edge of the reaction zone. This phenomenon may be associated with the buildup of substantial quantities of silicon in the iron, but a tendency toward wetting does seem to occur at higher temperatures in the driest atmospheres whether or not silicon enrichment occurs.

3. The particles give the general appearance of having been molten during the reaction, with smooth surfaces and a droplet-like shape which is very strongly suggestive of the molten state. Direct observations by Baker et al (1973, 1974, 1975), using reaction chambers have led them to state that the particles move in such a manner as to suggest that they are molten at temperature. This

is rather surprising because all temperatures used are well below the melting point of the iron-carbide eutectic.

4. Attempts to make quantitative measurements of channeling rates have not been particularly successful; certainly the rates vary by less than a factor of 20 from the lowest to the highest reaction temperatures. This relatively small change in reaction rates is consistent with a rather low activation energy ($\sim$10 kcal) for this reaction as has been reported by others.

5. Preliminary gas analyses have confirmed the presence of methane during reaction in dry hydrogen in keeping with expectations from published studies of hydrogenation reactions.

Modelling of Channeling Reactions

There are two major aspects to theoretical modelling of the kinetics of gasification reactions. The first is the local reaction mechanism at the point of carbon removal and the second is the transport of reactants and products and heat to and from the site of reaction. Depending on the relative rates, one or the other of these aspects may be the factor controlling the overall reaction rate. It is very difficult to take the transport factor into account in bulk samples with complicated morphologies, but for a simple structural feature such as a reaction channel in graphite we shall see that it is much easier. For a particular structural

feature in graphite the nature of the active carbon sites is quite well defined by the crystal structure. This, combined with the more easily characterizable transport aspects of the reaction, makes more precise modelling of the local reaction mechanism possible.

There is a good deal of controversy regarding the details of the mechanism of uncatalyzed reaction [see von Freddersdorf and Elliott (1966) for review] and this is even more true of the catalyzed reactions [see, for example Walker, Shelef and Anderson (1968)]. In many studies experiments were designed to eliminate transport aspects, or at least to verify that these aspects were not rate-limiting. The data from such experiments can be used to test purely local reaction mechanisms. This approach is likely to be more useful for the uncatalyzed reactions than the catalyzed reactions because the much higher reaction rates of the latter make transport control more likely. To illustrate the way in which models can be used to interpret data, we will examine a simple nontransport limited mechanism for the uncatalyzed reaction, and both the transport and local aspects of a tentative mechanism for the catalyzed reaction.

(1) The Uncatalyzed Reaction. The most reactive carbon atoms are atoms that have fewer than three nearest neighbors in the basal plane. Such active carbon atoms occur at defects such as nonbasal dislocations etc., but of more particular interest are active atoms at the edges of the basal atomic planes which occur at the risers of surface steps. The relatively large separation of

basal atomic planes makes it likely that reactions at the edge of each basal plane are independent of each other so that one can focus attention on a single basal plane edge when discussing mechanisms. The mechanism we shall discuss is a version of one proposed by Strickland-Constable (1950). There have been other, perhaps more plausible, mechanisms proposed [see von Feddersdorf and Elliott (1966)] but this mechanism has the virtue of simplicity for illustrating the points we wish to raise.

The mechanism is written in two steps

$$2Ca + H_2O \underset{j_1}{\overset{i_1}{\rightleftharpoons}} C(O) + H_2 + Ca \qquad (1)$$

$$C(O) \overset{i_2}{\rightleftharpoons} CO + nCa \qquad (2)$$

This reaction is illustrated for a "zig-zag" edge, i.e., an edge on a $(1\bar{1}01)$ step, in Figure 18. In the equations Ca is an active carbon site and C(O) is a C-O complex. In this mechanism we are assuming that the coverage of chemisorbed hydrogen and hydroxyl is negligible so that the intermediate steps in step 1 illustrated in Figure 18 are very fast. The inhibiting effect of H_2 on the reaction is due to the reverse of reaction (1) occurring at an appreciable rate. Others have taken the inhibiting effect of H_2 as due to the competitive adsorption of H_2 to form C(H) complexes, which reduces the sites available for H_2O absorption.

The reaction chosen for analysis here is especially easy to handle mathematically because it is necessary only to consider coverage by C(O) complexes, rather than C(O), C(H) and C(OH) complexes, and this is the reason for choosing it. In the following [Ca] is the number of uncomplexed active carbon sites per unit length of basal plane edge and [C(O)] is a similar density of C(O) complexes. If N is the total density of active edge atoms, then N = [Ca] + [C(O)]. For a zig-zag basal plane edge, $N = 4.08 \times 10^7$ cm^{-1} but for an "armchair" basal plane edge $N = 5.65 \times 10^7$ cm^{-1}.

The rate of creation of C(O) complexes is

$$\frac{d[C(O)]}{dt} = i_1 P_{H_2O} [Ca]^2 - j_1 P_{H_2} [Ca][C(O)] - i_2 [C(O)]$$

or in terms of the fractional coverage by C(O), $\Theta = C(O)/N$,

$$\frac{d\Theta}{dt} = Ni_1 P_{H_2O} (1-\Theta)^2 - Nj_1 P_{H_2} \Theta(1-\Theta) - i_2 \Theta \qquad (3)$$

The condition for steady state is that this rate should vanish, so that a quadratic equation can be solved for Θ. The solution is

$$\Theta = \frac{(2aP_{H_2O} + bP_{H_2} + 1) - \sqrt{(bP_{H_2} + 1)^2 + 4i_2 aP_{H_2O}}}{2(aP_{H_2O} + bP_{H_2})} \qquad (4)$$

where $a = N(i_1/i_2)$ and $b = N(j_1/i_2)$. This solution can be examined in various limits to see what the reaction order is with respect to the partial pressure of water. For example, it is easy to show that (4) predicts a first-order reaction with respect to P_{H_2O} for large P_{H_2} and zero order for very small P_{H_2}. It is also possible to relate the activation energy for the overall reaction in these

limits to the activation energies of the individual steps. This is the type of experimental test that can be performed to deduce the reaction mechanism and the activation energies of the basic steps.

The integrated effect of the reaction in a bulk carbon sample, as opposed to the local reaction at a single well-defined structural feature in graphite, will probably have the same qualitative form as (4), but because of the great variety of possible active carbon sites the mechanism may not be as well defined as (1) and (2) although the "average reaction" will be similar. For this reason, for the analysis of bulk data there is little point in a very precise mathematical analysis and it is common to ignore aspects of the reaction which lead to a nonlinear equation for the coverage, Θ. In our example, if one ignores the necessity of having <u>two</u> vacant sites for the absorption of water in (1), and the necessity of having one vacant site next to the absorbed oxygen atom in the reverse reaction, one can replace (3) by

$$i_1 P_{H_2O}(1-\Theta) - j_1 P_{H_2}\Theta - i_2\Theta = 0$$

with a slight redefinition of i_1 and j_1. This has solution

$$\Theta = \frac{aP_{H_2O}}{1 + aP_{H_2O} + bP_{H_2}} \qquad (5)$$

where $a = (i_1/i_2)$, $b = (j_1/i_2)$, which has exactly the Langmuir form. For both the exact and approximate treatments, the rate of carbon removal is

$$r_i = Ni_2\Theta,$$

and for the Langmuir form

$$r_i = \frac{Ni_1 P_{H_2O}}{1 + aP_{H_2O} + bP_{H_2}} \qquad (6)$$

Expressions of this form are often fitted to bulk kinetic data, and the activation energies for the rate-limiting reactions can be deduced from the parameters corresponding to the best fit [see von Freddersdorf and Elliott (1966)]. In principle this can also be done for the refined version of the solution. It is always possible to check the activation energies of the rate-limiting reactions in a mechanism by noting that the difference between the activation energy for the forward and the reverse reaction is just the heat of reaction, i.e., $E_f - E_r = \Delta H$. This is an especially useful procedure for reactions at crystallographically well-defined features on graphite because one has a fairly good idea of structure and can use standard bond energies to estimate ΔH.

A similar analysis has been carried out by Zeilke and Gorin (reviewed by von Freddersdorf and Elliot, 1966) for hydrogenation of graphite to form methane as illustrated schematically in Figure 19. Calculations of relative reaction rates using constants (a,b) derived from these models suggest that the hydrogenation reaction should be much more important in the temperature and atmosphere conditions used in this investigation.

(2) The Catalyzed Reaction. The much higher reaction rate for the catalyzed reaction makes it likely that transport phenomena play an important role in the mechanism. We shall study a particular hypothetical reaction mechanism which we are attempting to test with our data. We shall derive some observable consequences of the mechanism to see whether they are consistent with our data, or use the predictions to suggest further experiments. The modelling is still in its earliest stages and the following should be considered a first working hypothesis.

The only catalytic reaction mode we will consider is channeling of iron particles parallel to the basal plane of graphite. There are several qualitative observations which we would like the model to account for:

(i) Channels due to smaller diameter particles seem to be longer.

(ii) The iron particles appear to have been molten, even at reaction temperatures as low as 800°C.

(iii) The molten iron has a strong affinity for (wets) the risers of steps on the graphite surface.

(iv) Channels become wider (for the same depth) as P_{H_2O} gets smaller.

The mechanism we shall examine the consequences of is the following:

$$C(\text{graphite}) \rightarrow C(\text{in Fe}) \quad (7)$$

$$C(\text{in Fe}) \rightarrow Fe^*(C) \text{ (surface carbide)} \quad (8)$$

$$3Fe^* + H_2O \rightarrow Fe^*(O) + 2Fe^*(H) \quad (9)$$

$$Fe^*(C) + Fe^*(O) \rightarrow 2Fe^* + CO \quad (10)$$

$$2Fe^* + H_2 \rightarrow 2Fe^*(H) \quad (11)$$

$$C_{basal} + Fe^*(H) \rightarrow C_{basal}(H) + Fe^* \quad (12)$$

With reference to the sketch in Figure 17A and Figure 20, carbon atoms dissolve rapidly in iron at the graphite step [Eq. (7)], the carbon atoms then diffuse through the iron to the surfaces exposed [Eq. (8)]. At the same time, water is dissociatively adsorbed onto the iron [Eq. (9)]. The surface oxide and carbide then react to evolve carbon monoxide [Eq. (10)]. The adsorbed hydrogen atoms on the iron diffuse onto the graphite basal plane surface where they are highly mobile [see Robell, Ballore and Boudart (1964)]. These mobile hydrogen atoms recombine on remote iron particles which are not directly catalyzing a reaction (i.e., are not wetting a step). There is a net chemical driving force for surface diffusion of hydrogen atoms from actively catalyzing iron particles to inactive particles. Inactive particles may also act as sinks for atomic hydrogen generated in the uncatalyzed reaction.

We postulate the role of the mobile atomic hydrogen for three reasons:

(i) The evidence of Robell et al. (1964).

(ii) The fact that the iron at the channel tips appears molten in spite of the fact that the total reaction $C + H_2O \rightarrow CO + H_2$ is endothermic (ΔH = 31 kcal/mole). A possible explanation is that the partial reaction $3C + H_2O \rightarrow CO + 2C(H)$ is exothermic and localized at the reaction site, whereas the endothermic desorption step, $2C(H) \rightarrow 2C + H_2$ is delocalized. Since the heat of reaction for the total reaction is 31 kcal/mole, the heat of reaction for the local reaction is

$$\Delta H_{local} = 31 + E_{H-H} - 2E_{C-H} \text{ kcal/mole}$$

Now E_{H-H} = 103 kcal/mole, and E_{C-H} for carbon on active carbon sites at edges of the basal planes is 99 kcal/mole. The hydrogen atoms bonded to active carbons are immobile so these are not the hydrogens of interest. The hydrogen atoms of interest are bonded to basal plane surfaces and almost certainly $E_{C-H} \leqslant 99$ kcal/mole. There is a considerable amount of uncertainty about the value for E_{C-H}, but some estimates have been made. An experimental estimate, which should be more reliable than estimates from molecular orbital calculations [by Bennett, McCarroll, Messmer, (1971)], by Robell et al. (1964) is E_{C-H} = 68 kcal/mole, which makes the local reaction slightly exothermic $\Delta H_{local} \simeq -2$ kcal/mole.

(iii) Observations at sites where the uncatalyzed and catalyzed reactions are remote from large particles of iron, but

obviously associated with the large iron particles. The large iron particles may be recombination centers for atomic hydrogen.

The consequences of the local reaction mechanism can be worked out in a manner similar to that illustrated above for the uncatalyzed reaction, but for simplicity of illustration we shall assume a very simple local rate law at the surface of the iron:

$$J = k[C]_s P(s) \qquad (13)$$

where J is the rate of carbon removal (moles/cm^{2}s), $[C]_s$ is the surface carbon concentration, and P(s) is the partial pressure of water at the surface. We choose (13) because McKee (1974) indicates that Eq. (9) is the rate limiting step in the local mechanism. McKee (1974) also notices a reduction in activation energy above about 750°C which indicates a transition to diffusion control. This suggests that diffusion in the gas phase and/or iron and/or surface diffusion must be taken into account as possible rate-limiting steps. We shall assume that dissolution of graphite in iron, surface diffusion of atomic hydrogen, and recombination and dissociation of hydrogen are all fast reactions.

The steps that we shall consider as possibly rate-limiting are (i) the dissociation of water on the iron [after McKee (1974)], (ii) diffusion of gas-phase reactants and products to and from the iron surface (for the rate law of Eq. (13), only diffusion

of water vapor is of significance), (iii) diffusion of carbon through the iron. We shall assume that the water vapor must diffuse through a surface boundary layer of thickness δ, so that

$$J = k[C]_s p(s) = (\rho D/\delta)[p-p(s)]$$

where ρ is the molar density (moles/cm^3) of the gas, D is the diffusion coefficient of H_2O in the gas phase (cm^2/s), and p is the bulk gas-phase water partial pressure. Equation (14) can be solved for p(s) and the result can be substituted into (13) yielding

$$J = \frac{k[C]_s p}{1 + (k\delta/\rho D)[C]_s} \tag{15}$$

Now the problem is to solve the boundary-value problem of diffusion in the iron particle by adjusting $[C]_s$ at the surface so that J predicted by the boundary-value problem agrees with (15). This is a very difficult mathematical problem, so in the spirit of the approximations made so far, we make a further approximation which should still give a qualitative picture of the phenomenon.

Assume that there is no flux out of the top surface of the iron (or in the bottom surface). Then the flux is given by

$$J = (D'/w)([C]_e - [C]_s) \tag{16}$$

where D' is the diffusion coefficient of carbon in iron, w is the length of the iron particle, and $[C]_e$ is the equilibrium concentration of iron at the iron-carbon interface BC. Combination of (15) and (16) yields an equation which can be solved for $[C]_s$ yielding

$$C = \frac{1}{2}\{(1-b-arp) + [(1-b-arp)^2 + 4b]^{1/2}\} \tag{17}$$

where $C = [C]_s/[C]_e$, $r = w/d$, $a = \frac{\rho D d}{[C]_e D' \delta}$, $b = \frac{\rho D}{k\delta[C]_e}$ (18)

Figure 20 is a plot of c vs arp for several values of b. There are three possible regimes:

(i) Local control: $b>>1$, $b/(arp)>>1$

(ii) Gas-phase diffusion control $arp<<1$, $b<<1$

(iii) Bulk (iron) diffusion control $arp>>1$, $b/(arp)<<1$.

The total gasification rate in moles per second per unit length of step is Q and

$$q = \frac{Q}{k[C]_e pd} = \frac{bc}{b + c} \tag{19}$$

For small values of b and sufficiently small values of w (gas phase limited), the rate of gasification approaches a limiting value. If one takes into account the gas phase diffusion-limited flux through the top surface of the iron particle and takes note of the fact that in this regime the total gasification rate should be proportional to the exposed area of the particle, then this limiting value will actually be a maximum at a finite value of w. This

crude model predicts that in this regime this maximum will occur at arp = constant. Thus the temperature and water-vapor pressure dependence of the width of iron strips wetting steps on the graphite surface would be a useful way to test this model (or a more rigorous version of it).

A particularly striking phenomenon in the catalyzed reaction is the "channelling" of small iron particles on the basal plane surfaces. The iron particles cut grooves in the surface, and it appears that the smaller the particle, the longer the groove. Let us consider particles small enough that diffusion of carbon through the iron is not limiting. A particle of radius R cuts a groove of depth 2R as it moves across the surface, and heating due to the local exothermic reaction causes a local temperature rise ΔT. It is easy to demonstrate that the primary heat-loss mechanism is by conduction into the graphite, and that the total heat loss rate is (cal/sec)

$$Q = 2\pi\kappa\Delta TR \tag{20}$$

where κ is the thermal conductivity of graphite, assumed isotropic. A similar treatment of Fick's law gives the total molar gasification rate as (moles/sec).

$$G = 2\pi\rho D[p(s)-p]R \tag{21}$$

If the local heat of reaction is ΔH (<0 for exothermic), then

$$Q = G\Delta H \tag{22}$$

If diffusion through iron is not rate-limiting, then the local reaction rate law can be written

$$G = k_1 p(s) \tag{23}$$

where, in terms of the k defined earlier

$$k_1 = k[C]_e A \tag{24}$$

where A is the exposed area of the iron particle ($\sim 2\pi R^2$). Equations (21) and (23) may be combined and solved for p(s) which may then be substituted into (23) to give

$$G = p \left\{ \frac{1}{k_1} + \frac{1}{2\pi\rho DR} \right\}^{-1} \tag{25}$$

On the other hand, G must be related to the velocity v by

$$G \simeq v\rho' \pi R^2 \tag{26}$$

where ρ' is the molar density of graphite. So, from (25) and (26)

$$v = p \left\{ \frac{\pi\rho' R^2}{k_1} + \frac{\rho' R}{2\rho D} \right\}^{-1} \tag{27}$$

Thus, for local control v varies as $1/R^2$, but for diffusion control v varies as 1/R. All parameters except k_1 in (27) are known or easily measured. Thus velocity measurements can in principle yield information about the local rate constant k_1. At sufficiently high temperatures the reaction must become diffusion controlled and thus insensitive to k_1 because k_1 has an Arrhenius dependence on T, whereas D varies only as $T^{3/2}$. It is also possible to find the local temperature rise via (20), (22) and (25):

$$\Delta T = \frac{p\Delta H}{\kappa} \left\{ \frac{2\pi R}{k_1} + \frac{1}{\rho D} \right\}^{-1} \qquad (28)$$

Thus, in the diffusion-controlled regime ΔT is independent of particle size, but for local control, smaller particles get hotter. It is useful to compute v and ΔT in the diffusion controlled regime, because these values constitute upper limits on v and ΔT. In the diffusion controlled regime, one finds ΔT is at most only a couple of degrees, whereas v is on the order of 10 cm/s for a 1000 Å particle. The small value of ΔT seems to contradict the fact of molten iron particles, whereas the large value of v seems to contradict the observed finite track lengths. These contradictions suggest that a further refinement of the model, perhaps taking alternative diffusion paths into account, will be necessary.

None of the above analysis is intended as a definitive model of the reaction mechanism. The intention is rather to show how a mechanism may be proposed as a plausible working hypothesis, how its consequences may be evaluated, and how, in conjunction with experimental results, it may be used to suggest definitive measurements.

Future Research

The areas of investigation that will be explored further either during the remaining period of the present contract or during the continuation year if this is approved are listed below in approximate order of priority.

1. The origin of the silicon impurity must be identified and its influence on reaction rates and nature of the reaction channels determined.

2. Quantitative measurements of the various characteristics of the reaction channels will be carried out using available instrumental stereo viewing facilities. That is, the length, width, depth, crystallographic orientation and number of jogs per unit length will be determined on representative samples, and correlated with reaction temperature, gas atmosphere, reaction products (i.e., CO and CH_4) and catalytic particle size. There is some difficulty in these measurements because of interference of tracks with one another. Efforts will be made to minimize this difficulty by reducing the density of catalytic particles on the graphite surface. Although controlling particle size and number per unit area independently does not appear to be easy, some preliminary experiments employing masks during vacuum deposition suggest that this approach might be satisfactory. The MVEM and SEM observations suggest that the characteristics of the track do depend on particle size. That is, channels formed by very large particles protruding above them tend to change in direction and width frequently possibly because of vibration causing a wobbly motion whereas the very small particles completely immersed in the track are not affected and the tracks tend to remain very straight.

3. An environmental reaction chamber for the million volt electron microscope will be ready shortly and it is anticipated that this will prove to be a more satisfactory way of obtaining quantitative reaction data. That is, the rate of advance of individual channels can be measured directly, and sources of interference eliminated by watching channel growth over a relatively short period of time and distance.

4. Additional effort will go into attempts to identify the unknown phase which forms at high temperatures and which possibly is an iron-silicon carbide.

5. Preliminary measurements of the gas composition will be extended for other reaction temperatures and other atmospheres to determine the relative production of CH_4 and CO during gasification of electrode graphite. If sensitivity of the instrumentation can be increased efficiently, similar measurements will be made on selected flakes of single crystal graphite. Quantitative information on the relative gasification rates will be correlated with the nature of the reaction channels to substantiate some indication that channel orientation is different for hydrogenation and oxidation reactions.

6. The appearance of the particles and comments reported in the literature by Baker et al, and others strongly suggest

that the iron particles are molten during the reaction. As discussed in the theoretical section of this report, the temperature rise of the reaction is negligible, at least according to the model developed here. Direct methods to determine the phase present at the reaction temperature will be attempted using Mossbauer spectroscopy, magnetic measurements, x-ray diffraction, or electron diffraction at the reaction temperature.

7. Considerable effort will go into theoretical modelling of the various observations that have been made during the course of this research. One aspect concerns the crystallography of the removal of carbon atoms from the graphite lattic and particularly the nature of the exposed surfaces. As discussed in the text, models that have been presented for the CO and CH_4 reactions assume either $\langle 11\bar{2}0 \rangle$ or $\langle 1\bar{1}10 \rangle$ exposed edges, respectively. However the observations tend to suggest that just the reverse is true.

8. Some preliminary thermodynamic calculations will be extended to compute an iron-carbon phase diagram on the assumption that austenite does not occur. Nucleation of new phases in very small particles is well known to be difficult and it is possible here that the iron particles do not form fcc austenite but remain as bcc ferrite. It is probable that if this situation actually occurs, the metastable extension of the eutectic temperature will

result in a substantial lowering of the melting point and explain the apparent molten appearance of the particles.

9. Electron microscope examination of samples reacted at high temperature in wet H_2 shows that the edges of the reaction channel have a very ragged appearance. Presumably this is due to noncatalytic reactions, and the conditions that affect this will be explored in more detail.

10. The effect of other catalytic materials will be explored, including nickel, copper, and gold because of substantially different chemical equilibria of these materials with carbon.

11. Surface-energy considerations affecting particle shape and particle movement will be examined. Forces causing movement of particles either over the surface during the reduction stage or along the channels during the gasification reaction are physical-chemical in nature and the magnitude of these forces will be evaluated theoretically.

References

Theory and Fundamental Mechanisms

1. Abrahamson, J., "The Surface Energies of Graphite Carbon," 11, 337-362, (1973).

2. Baltzold, R. C., and Somerjai, G. A., "Pre-exponential Factors in Surface Reactions," J. Catalysis, (1976).

3. Bennett, A. J., McCarroll, B., and Messmer, R. P., "A Molecular Orbital Approach to Chemisorption I - Atomic Hydrogen on Graphite," Surface Science, 24, pp. 191-208, (1971).

4. Bennett, A. J., McCarroll, B., and Messmer, R. P., "Molecular Orbital Approach to Chemisorption II - Atomic H, C, N, O, and F on Graphite," Phys. Rev. B3, 1397, (1971).

5. Bond, G. C., "Catalysis by Metals," Academic (1962).

6. Boudart, M., Delbouille, A., Dumesic, J. A., Khammooma, S., and Topsøe, H., "Surface, Catalytic and Magnetic Properties of Small Iron Particles - 1. Preparation and Characterization of Samples," J. Catalysis 37, pp. 486-502 (1975).

7. Dumesic, J. A., Topsøe, H., and Boudart, M., "Surface, Catalytic and Magnetic Properties of Small Iron Particles III - Nitrogen Induced Surface Reconstruction," J. Catalysis 37, pp. 513-522 (1975).

8. Dumesic, J. A., and Topsøe, H., Khammooma, S., and Boudart, M., "Surface, Catalytic and Magnetic Properties of Small Iron Particles II - Structure Sensitivity of Ammonia Synthesis," J. Catalysis 37, pp. 503-512 (1975).

9. Ergun, S., and Menster, M., "Reactions of Carbon With Carbon Dioxide and Steam," in "Chemistry and Physics of Carbon," Vol. 1, p. 203, (1965).

10. Feates, F. S., Harris, P. S., and Reuben, B. G., "Compensation Effect in the Kinetics of the Catalyzed Oxidation of Carbon," Journal of the Chemical Society, Faraday Transactions I, 2011 (1974).

11. Fowler, R. H., "A Statistical Derivation of Langmuir, Absorption Isotherm," Proc. Canb. Phil. Soc. 31, 260 (1935).

12. Glasstone, S., (Laidler, K. J. and Eyring, H.) "The Theory of Rate Processes," McGraw-Hill (1941).

13. Harris, P. S., "Correlations in the Catalytic Activity of Metals in the Graphite-Oxygen Reaction," Carbon 10, 643 (1972).

14. Hayward, D. O. (and Trapnell, B. M. W.), "Chemisorption," Butterworths, Washington, (1964).

15. Langmuir, I., "The Absorption of Gases on Plane Surfaces of Glass, Mica and Platinum," J. Amer. Chem. Soc. 40, 1361-1403 (1918).

16. Messmer, R. P., and Bennett, A. J., "Orbital Symmetry Rules for Chemisorption and Catalysis," Physical Review B 6, 633 (1972).

17. Thring, M. W. (and Essenhigh, R. H.), "Thermodynamics and Kinetics of Combustion of Solid Fuels," in "Chemistry of Coal Utilization," edited by H. H. Lowry, Wiley (1967).

18. von Freddersdorf, C. G. (and Elliott, M. A.), "Coal Gasification," in "Chemistry of Coal Utilization," Supplementary Volume, edited by H. H. Lowry (Wiley, 1966), pp. 892-1022.

19. "Bulk Studies of Carbon-Gas Reactions," Binford, J. S. and Eyring, H., "Kinetics of the Steam-Carbon Reaction," J. Phys. Chem. 60, 486 (1956).

20. Blyholder, G., Binford, J. S., Jr., and Eyring, H., "A Kinetic Theory for the Oxidation of Carbonized Filaments," J. Phys. Chem. 62, 263-267 (1958).

21. Blyholder, G., and Eyring, H., "Kinetics of Graphite Oxidation," J. Phys. Chem. 61, 682-688 (1957).

22. Blyholder, G., and Eyring, H., "Kinetics of the Steam-Carbon Reaction," J. Phys. Chem. 63, 693-693 (1959).

23. Gadsby, J., Hinshelwood, C. N., and Sykes, K. W., "The Kinetics of the Reactions of the Steam-Carbon System," Proc. Roy. Soc (Lond.) A187, 129-151 (1946).

24. Long, F. J., and Sykes, K. W., "The Catalysis of the Carbon Monoxide-Steam Reaction," Proc. Roy. Soc. (London) 215A, 111-119 (1952).

25. Long, F. J., and Sykes, K. W., "The Catalysis of the Oxidation of Carbon," J. Chim. Phys. 47, 361-378 (1950).

26. Long, F. J., and Sykes, K. W., "The Effect of Specific Catalysts on the Reactions of the Steam-Carbon System," Proc. Roy. Soc. (London) A215, 100-110 (1952).

27. Marsh, H. (Foord, A. D.), "Mechanisms of Oxidation of Carbon by Molecular Oxygen," Carbon 11, 421 (1973).

28. McKee, D. W., "The Copper Catalyzed Oxidation of Graphite," Carbon 8, 131-139 (1970).

29. McKee, D. W., "Effect of Metallic Impurities on the Gasification of Graphite in Water Vapor and Hydrogen," Carbon 12, 453-464 (1974).

30. McKee, D. W., "Metal Oxides as Catalysts for the Oxidation of Graphite," Carbon 8, 623-635 (1970).

31. Phillips, R. (Vastola, F. J. and Walker, P. L.), "Kinetics of the Carbon-Carbon Dioxide Reaction Under a Continuous Linear Temperature Increase," Carbon 14, 83 (1976).

32. Rellick, G. S. (F. Rodriguez-Reinoso, P. A. Thrower and P. L. Walker), "Transient Rates in the Reaction of CO_2 With Highly Oriented Pyrolytic Graphite," Carbon 13, 81-82 (1975).

33. Rellick, G. S. (P. A. Thrower and P. L. Walker), "Oxidation of Compressed Annealed Pyrolytic Graphites," Carbon 13, 71-80 (1975).

34. Strickland-Constable, R. F., J. Chim. Phys. 47, 356 (1950).

35. Turkdogan, E. T. (and Vinters, J. V.), "Catalytic Oxidation of Carbon," Carbon 10, 97-110 (1972).

36. von Freddersdorf, C. G. (and Elliott, M. A.), "Coal Gasification," in "Chemistry of Coal Utilization," Supplementary Volume, edited by H. H. Lowry (Wiley, 1966), pp. 892-1022.

37. Walker, P. L. (and Shelef, M. and Anderson, R. A.), "Catalysis of Carbon Gasification," in "Chemistry and Physics of Carbon," Vol. 4, p. 287 (1968).

Microscopic Studies of Graphite-Gas Reactions

1. Baker, R. T. K (and P. S. Harris), "Controlled Atmosphere Electron Microscopy Studies of Graphite Gasification I - The Catalytic Influence of Zinc," Carbon, 11, 25-31 (1973).

2. Baker, R. T. K. (Harris, P. S., Kemper, D. J., and Waite, K. J.), "Controlled Atmosphere Electron Microscopy Studies of Graphite Gasification - 3. The Catalytic Influence of Molybdenum and Molybdenum Trioxide," Carbon 12, 179-187 (1974).

3. Baker, R. T. K. (R. B. Thomas and M. Wells), "Controlled Atmosphere Electron Microscopy Studies of Graphite Gasification - The Catalytic Influence of Vanadium and Vanadium Pentoxide," Carbon 13, 141-145 (1975).

4. Fryer, J. R., "Oxidation of Graphite Catalyzed by Palladium," Nature 220, 1121 (1968).

5. Harris, P. S. (F. S. Feates, B. G. Reuben), "Controlled Atmosphere Electron Microscopic Studies of the Catalyzed Graphite-Oxygen Reaction 2. The Influence of Lead," Carbon 11, 565-566 (1973).

6. Harris, P. S. (F. S. Feates and B. G. Reuben), "Controlled Atmosphere Electron Microscopy Studies of Graphite Gasification - 4. Catalysis of the Graphite-O_2 Reaction by Silver," Carbon 12, 189-197, 1974.

7. Hennig, G. R., "Catalytic Oxidation of Graphite," J. Inorg. and Nucl. Chem., 24, 1962.

8. Hennig, G. R., "Emfluss von Gitterdefekten und Katalysatoren auf Oberflächen-reaktionen von Graphit-Einkristallen," Zeitschrift für Elecktrochemic, 66 629 (1962).

9. Hennig, G. R., "Electron Microscopy of Reactivity Changes Near Lattice Defects in Graphite," in "Chemistry and Physics of Carbon," Vol. 2, p. 1 (1966).

10. McCarroll, B. (and McKee, D. W.), "Reactivity of Graphite Surfaces With Atoms and Molecules of Hydrogen, Oxygen and Nitrogen," Carbon 9, 301 (1971).

11. O'Hair, T. E., "Graphite Oxidation - The Mobile Surface Oxide Intermediate," Carbon 7, 702 (1969).

12. Thomas, J. M., "Microscopic Studies of Graphite Oxidation," in "Chemistry and Physics of Carbon," Vol. 1, p. 122 (1965).

13. Thomas, J. M., "Topographical Studies of Oxidized Graphite Surfaces. A Summary of the Present Position," Carbon 7, 359, (1969).

General and Miscellaneous Properties of Graphite and Other Carbons

1. Abrahamson, J., "Graphite Sublimation Temperatures of Carbon Arcs and Crystallite Erosion," Carbon 12, 111-141 (1974).

2. Baker, C. (and Kelly, A.), "Energy to Form and to Move Vacant Lattice Sites in Graphite," Nature 193, 235 (1962).

3. Barton, S. S. (and Harrison, B. H), "Acidic Surface Oxide Structures on Carbon and Graphite - I," Carbon 13, 283 (1975).

4. Davis, T. F., "Graphite - A Selected Bibliography," U. S. Atomic Energy Commission, Report Number TID-3314 (Physics) (1962).

5. Freise, E. J. (and A. Kelly), "Twinning in Graphite," Proc. Roy Soc. A264, 269 (1961).

6. Montet, G. L., "The Threshold Curve for the Displacement of Atoms in Graphite," Carbon 11, 89-92, (1973).

7. Montet, G. L, "Threshold Energy for the Displacement of Atoms in Graphite," Carbon 5, 19-23 (1967).

8. Montet, G. L. (and G. E. Meyers), "Threshold Energy for the Displacement of Surface Atoms in Graphite," Carbon 9, 179-183, (1971).

9. Omori, M. (T. Hirai, S. Yajima), "Electron Microscope Observation of Carbon Layers Around Iron Particles Dispersed in a Glasslike Carbon Matrix," Carbon 12, 474-476 (1974).

10. Reynolds, W. N., "Physical Properties of Graphite," Elsevier, (1968).

11. Robell, A. J., Ballou, E. V. and Boudart, M., "Surface Diffusion of Hydrogen on Carbon," J. Phys. Chem. 68, 2748 (1964).

12. Thomas, J. M. (and Roscoe, C.), "Nonbasal Dislocations in Graphite," in "Chemistry and Physics of Carbon," Vol. 3, p. 1 (1968).

13. Ubbelohde, A. R. (and Lewis, F. A.), "Graphite and Its Crystal Components," (Oxford, 1960).

14. Walker, P. L. (ed.), "The Chemistry and Physics of Carbon," Vol. 1.

Electron Microscopy Techniques

1. Baker, R. T. K. (and P. S. Harris), "Controlled Atmosphere Electron Microscopy," J. Phys. (E) 5, 793 (1972).

2. Cullis, A. G. (and Maher, D. M.), "High Resolution Topographical Imaging by Direct Transmission Electron Microscopy," Phil. Mag. 30, 447 (1974).

3. Cullis, A. G. (and Maher, D. M.), "Topographical Contrast in the Transmission Electron Microscope," Ultra Microscopy 1, 97 (1975).

4. Cullis, A. G. (Maher, D. M. and Nakahara, S.), "Topographical Imaging in the Transmission Electron Microscope," 33rd Ann. Proc. Electron Microscopy Soc. Amer., Las Vegas, Nevada (1975), G. W. Bailey (ed) p. 202.

5. Nakahara, S. (Cullis, A. G. and Maher, D. M.), "Theory of Topographical Image Contrast," 33rd Ann. Proc. Electron Microscopy Soc. Amer., Las Vegas, Nevada (1975), G. W. Bailey (ed) p. 188.

6. Nakahara, S. (Maher, D. M. and Cullis, A. G.), "Principle, Theory and Application of Topographical Image Contrast," Proc. 6th European Cong. on EM, Israel (1976).

Thermodynamic and Other Data Used in the Experimental Design

1. Baird, T., "Effect of Metals and Surface Contamination on the Decoration of Graphite," Carbon 12, 381 (1974), and J. R. Fryer and Arbuthnott, McAneney, Riddell, Walker - Decoration.

2. Baird, T. (J. R. Fryer, A. R. Arbuthnott, B. McAneney, E. V. Riddell, and D. Walker), "Effect of Metals and Surface Contaminants on the Decoration of Graphite," Carbon 12, 381-390 (1974).

3. Baron, R. E., Porter, J. H. and Hammond, O. H., Jr., "Chemical Equilibria in Carbon-Hydrogen-Oxygen Systems," The MIT Press, Cambridge, Mass. (1976).

4. Bromley, L. A., "Viscosity Behavior of Gases," Industrial and Engineering Chemistry 43, 1641 (1951). And C. R. Wilke, Representations of Viscosity Data.

5. Chipman, J. (and Marshall, S.), "The Equilibrium FeO + H_2 = Fe + H_2O at Temperatures up to the Melting Point of Iron," J. Am. Chem. Soc. 62, 299 (1940).

6. Darken, L. S. (and Gurry, R. W.), "Physical Chemistry of Metals," McGraw-Hill (1953).

7. Darken, L. S., "The System Iron-Oxygen I. The Wüstite Field and Related Equilibria," J. Am. Chem. Soc. 67, 1398 (1945), And R. W. Gurry.

8. Dastur, M. N. (and J. Chipman), "Elimination of Thermal Diffusion Error in Studies of Gas-Metal Equilibrium," Faraday Society Discussions, 4, 100-108 (1948).

9. Emmett, P. H. and Shultz, J. F., "Equilibria in the Fe-H-O System - Indirect Calculation of the Water Gas Equilibrium Constant," J. Am. Chem. Soc. 52, 4268 (1930).

10. Emmett, P. H. and Shultz, J. F., "Gaseous Thermal Diffusion - The Principal Cause of Discrepancies Among Equilibrium Measurements on the Systems Fe_3O_4-H_2-Fe-H_2O-Fe_3O_4-H_2-FeO-H_2O and FeO-H_2-Fe-H_2O," J. Am. Chem. Soc. 55, 1376-1384 (1933).

11. Powell, Carroll F. (ed), "Vapor Deposition," other eds. J. H. Oxley, J. M. Blocher, Jr., John Wiley and Sons, Inc., (1966). Has useful tabulation of metal/filaments for evaporation.

12. Richardson, F. D. and Jeffes, J. H. E., "Thermodynamics of Substances of Interest in Iron and Steel Making from o°C to 2400°C," Journal of the Iron and Steel Institute, 160, 261 (1948).

13. Seybolt, A. U. (and Burke, J. E.), "Procedures in Experimental Metallurgy," Wiley (1953).

14. Tombs, N. C. and Welch, A. J. E., "Thermodynamic Properties of Silicon Monoxide," Journal of the Iron and Steel Institute, 172, 69 (1952).

15. Wilke, C. R., "A Viscosity Equation for Gas Mixtures," J. Chem. Phys. 18, 517 (1950).

16. Tsederberg, N. V., "Thermal Conductivity of Gases and Liquids," MIT Press (1965). Translation by Scripta Technica.

Table I

Summary of Reaction Experiments

PH_2O Atm.	Temperature, °C 1100	1000	900	850	800	750	650
2-4 x 10^{-2}	(60)[3]			(47)	(22,23)	(41)	
2-4 x 10^{-3}		(49)	(33,44,45)	(32,46)	(28,29, 42,43)	(39,40)	(30)
2-4 x 10^{-4}	(51,52)	(50)		(48) (55)[1]	(27)		
2-4 x 10^{-5}	(53,54, 57,56)[2]	(63)		(31)	(21)	(24,25)	
2-4 x 10^{-6}		(58,62)	(59)				

Sample in ( ) Indicates Experiment No.

(55)[1] 80% He, 20% H_2

(56)[2] 90% He, 10% H_2

(60)[3] 100% He, 0% H_2

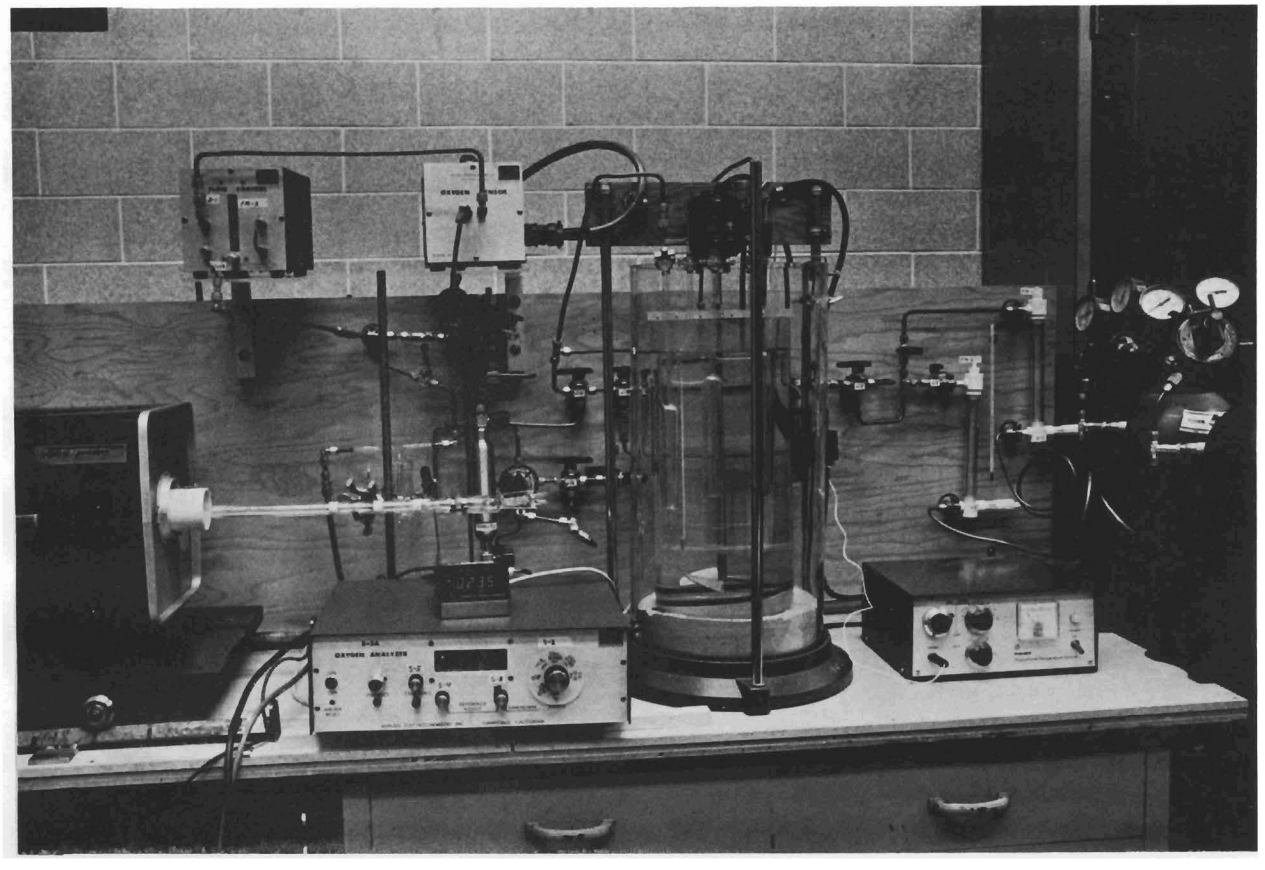

Photograph of gas flow controls, mixing and sampling units, furnace and oxygen sensor for carbon gasification experiments.

Figure 1

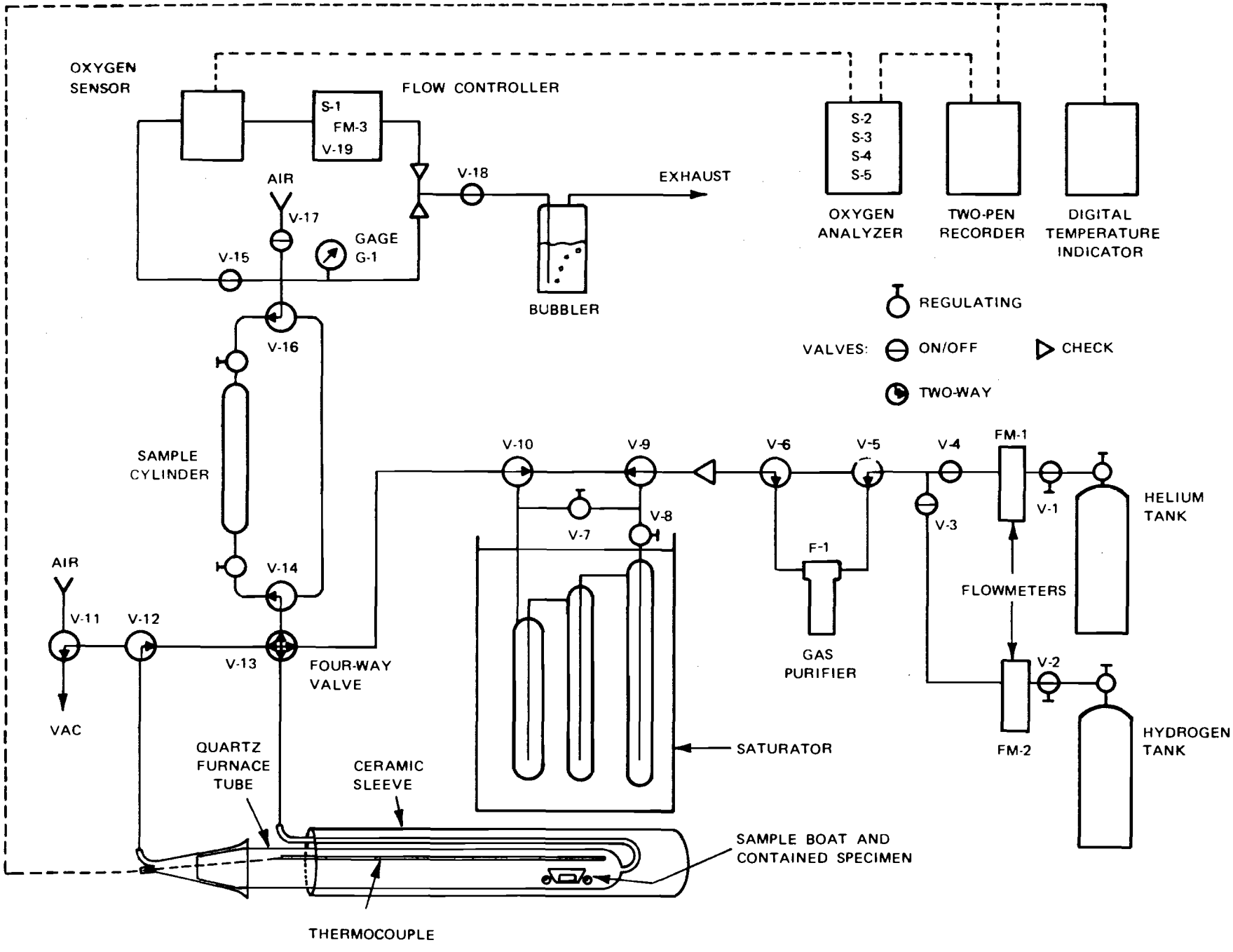

SCHEMATIC DRAWING OF GAS FLOW CONTROL, MIXING AND ROUGHING SYSTEM, OXYGEN SENSOR AND REACTION CHAMBER

76-H-025(064)

Figure 2

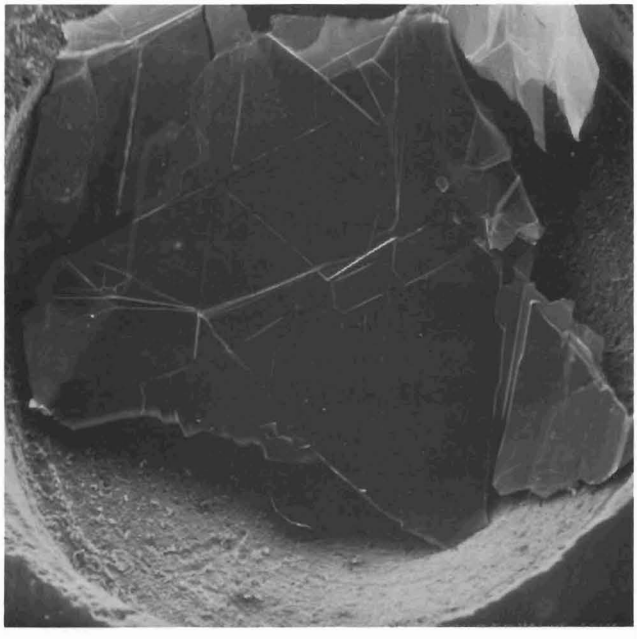

A 30X

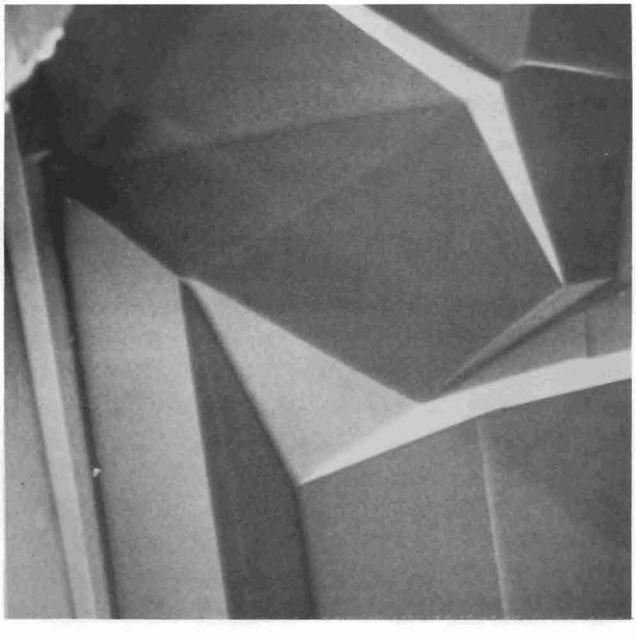

B 500X

Example of freshly cleaved graphite flakes used for reaction channeling experiments showing presence of twinned regions.

Figure 3

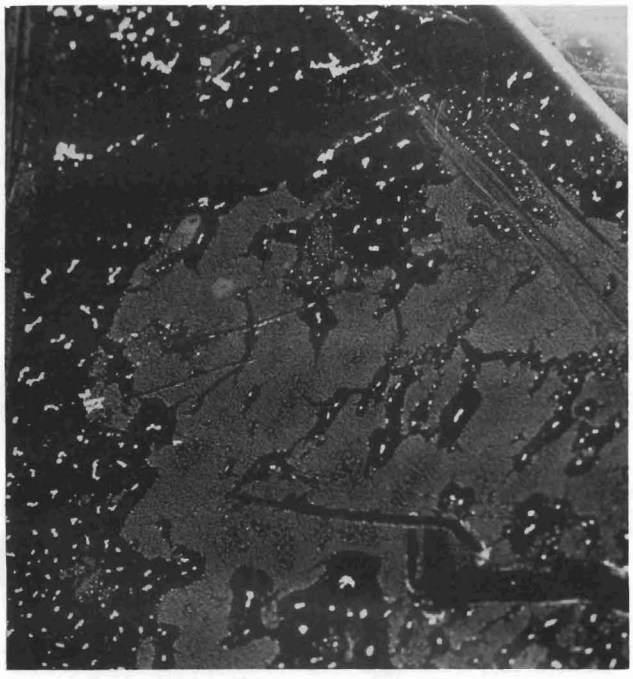

A 800X

B 8,000X

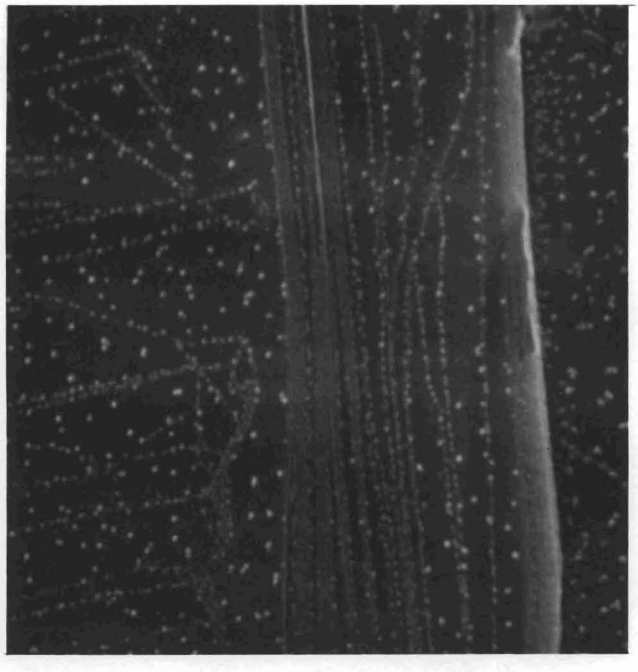

C 10,000X

D 4,000X

Examples of the various stages of the formation of small particles of metallic iron during heating in dry ($P_{H_2O}=10^{-5}$ atm) hydrogen at 750°C.
(A,B) ∿5nm film formed by vapor deposition breaks up into spherical particles; (C) decoration of surface ledges; (D) some particles enlarged by migration over smooth graphite surface.
Scanning Electron Micrographs

Figure 4

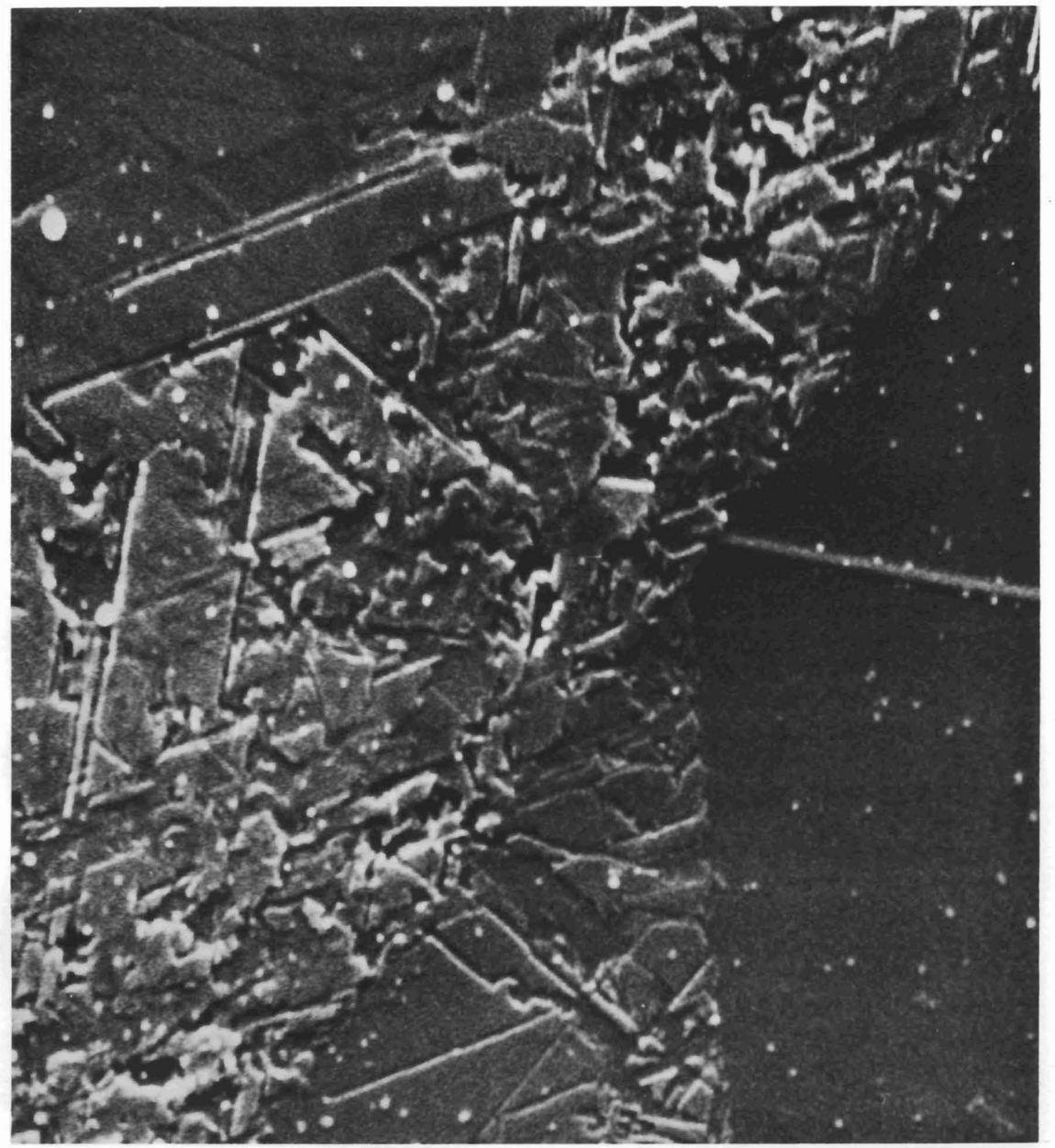

Iron particle catalyzed channeling is initiated at ledge on cleaved surfaces. Reacted 20 minutes in "wet" hydrogen at 800°C; $P_{H_2O}=3\times10^{-2}$ atm. Scanning Electron Micrograph 15,000X

Figure 5

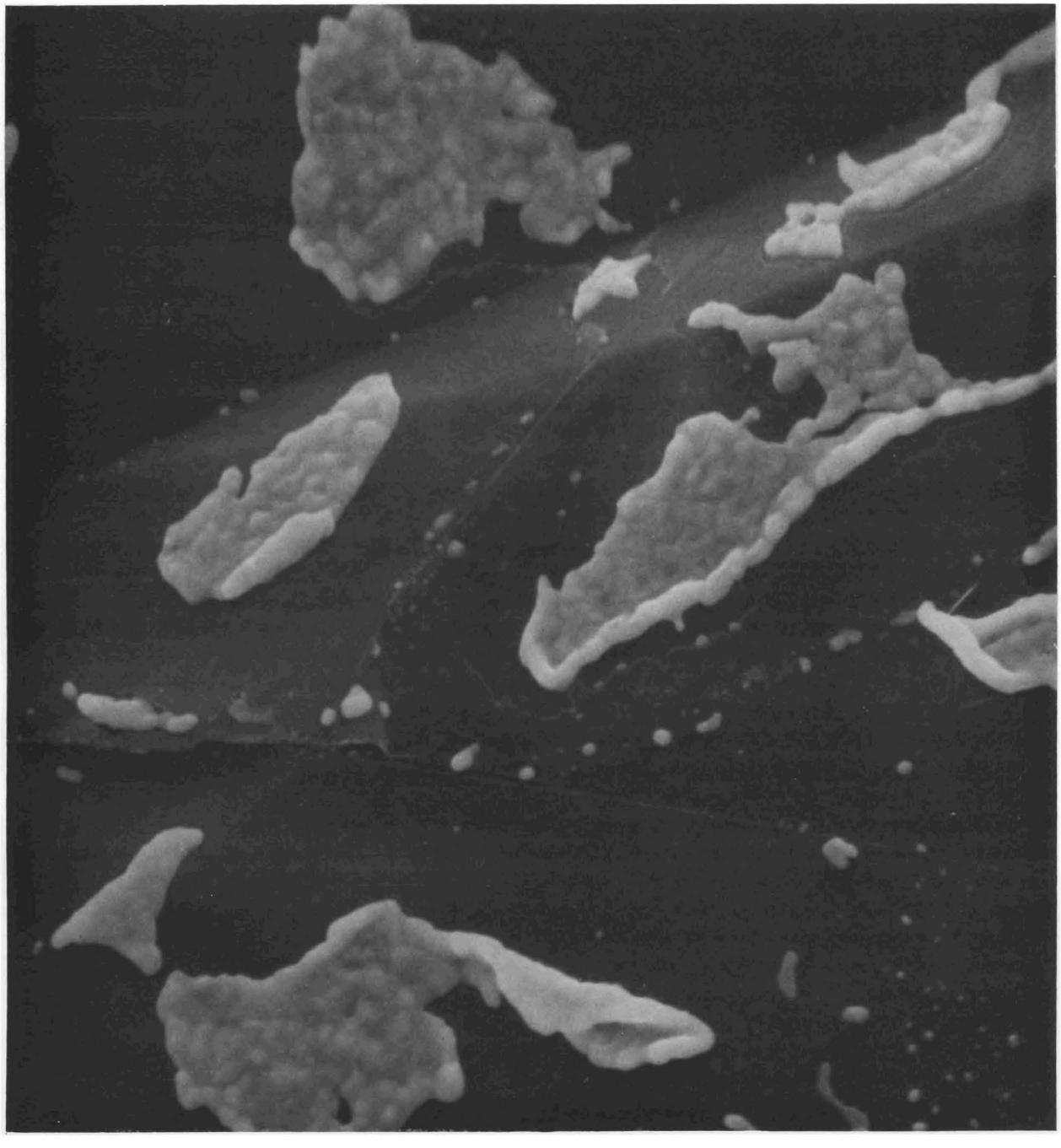

Reaction around large iron particles. Nominal 1000 Å layer of iron reduced in dry hydrogen for 90 min., then reacted in wet hydrogen for 20 min., both at 700°C. 4,500X
Scanning Electron Micrograph

Figure 6

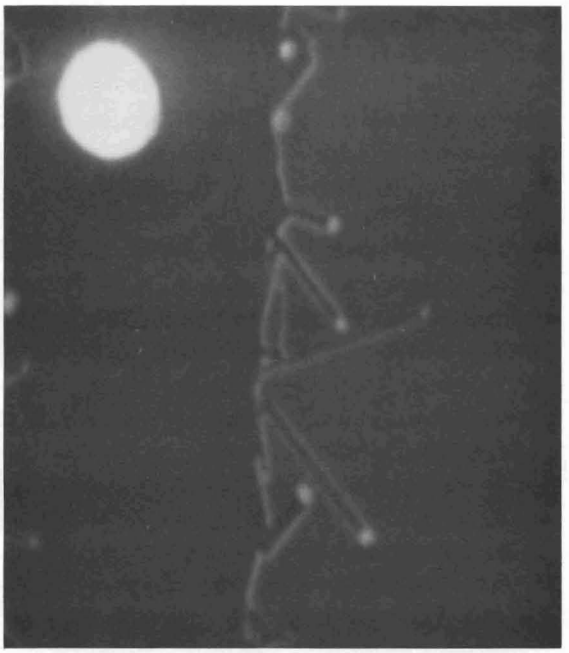

A 30,000X

B 8,000X

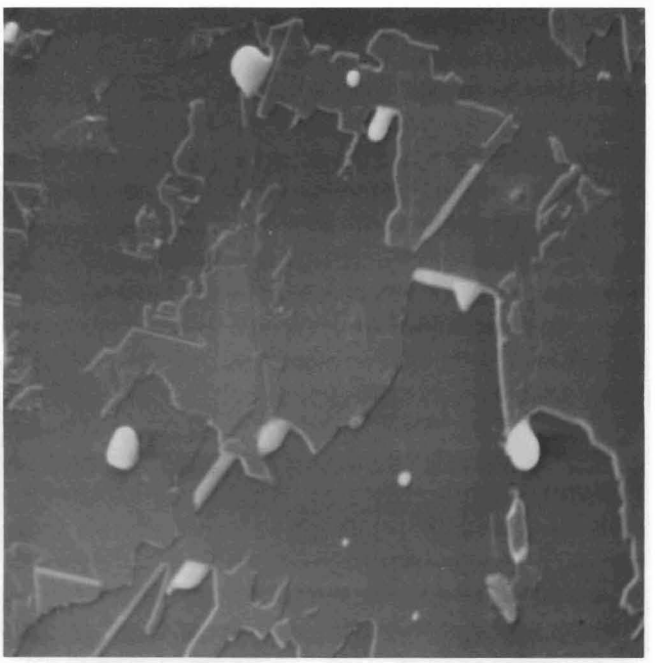

C 8,000X

Examples of reaction channels formed at different temperatures. (A) 800°C; $P_{H_2O}=4.5\times10^{-3}$. (B) 1000°C; $P_{H_2O}=4\times10^{-3}$. (C) 1100°C; $P_{H_2O}=1.37\times10^{-5}$ atm. Scanning Electron Micrograph

Figure 7

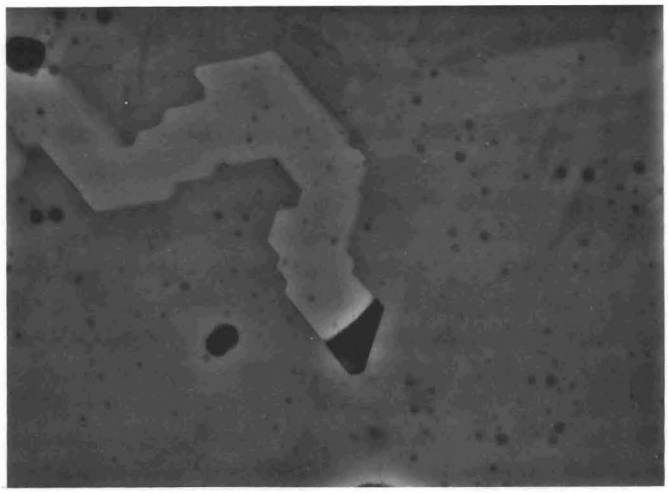

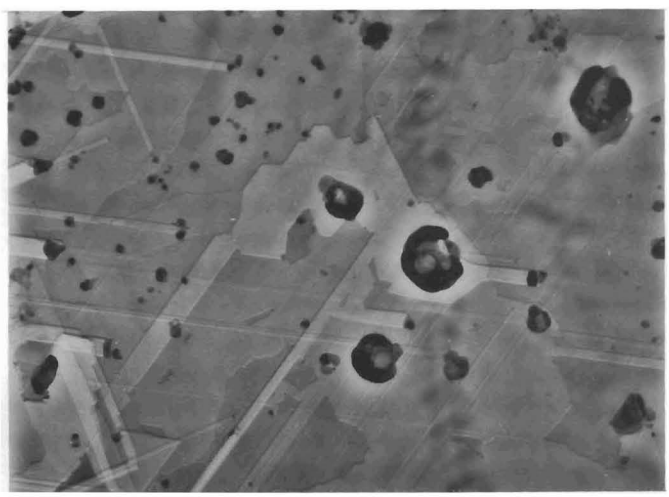

Examples of channels formed by movement of thin single crystal particles in 80%He, 20%H_2. 850°C; $P_{H_2O}=4\times10^{-4}$ atm. 23,500X

Million Volt Electron Micrographs

Figure 8

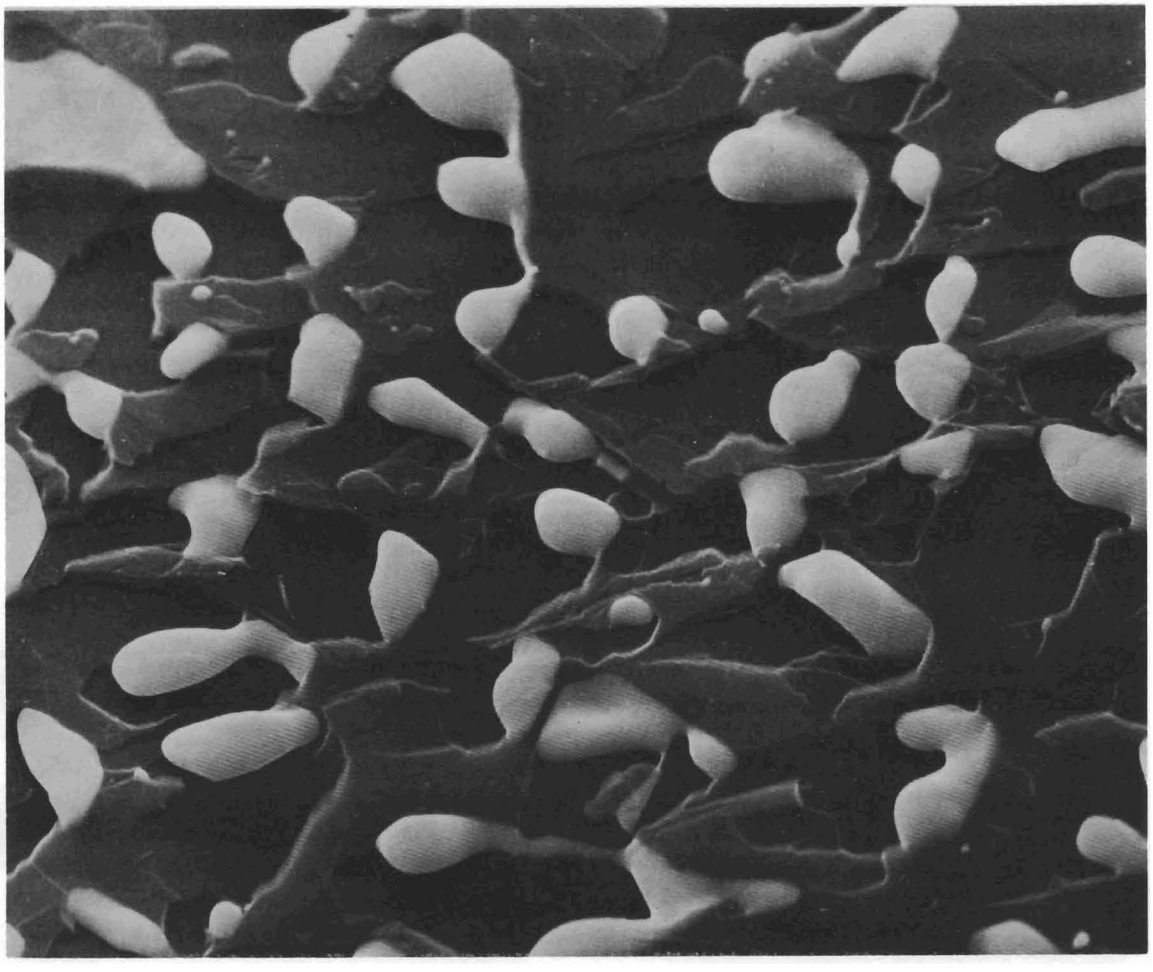

Reaction channels formed at 1000°C in dry hydrogen with 1000 Å of iron. 1000°C; P_{H_2O}=1.3x10^{-5} atm. 8,000X Scanning Electron Micrograph

Figure 9

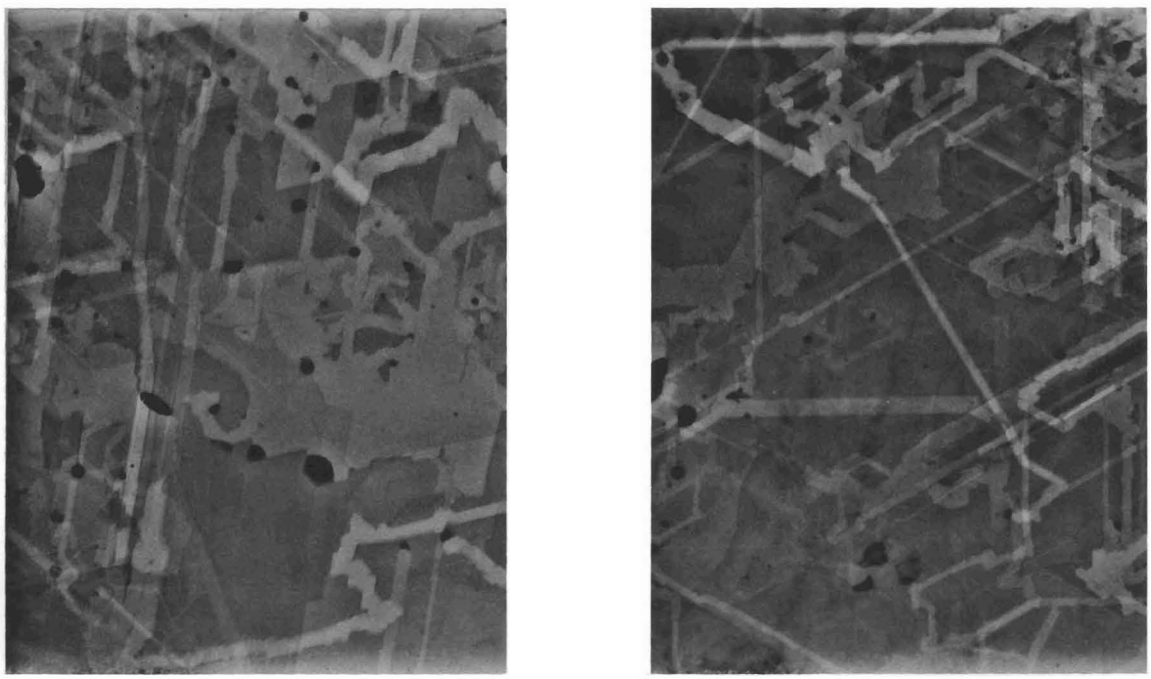

Iron particle catalyzed reaction channels formed at 1100°C; $P_{H_2O}=4.14\times10^{-4}$ atm. 15,000X
Million Volt Electron Micrographs

Figure 10

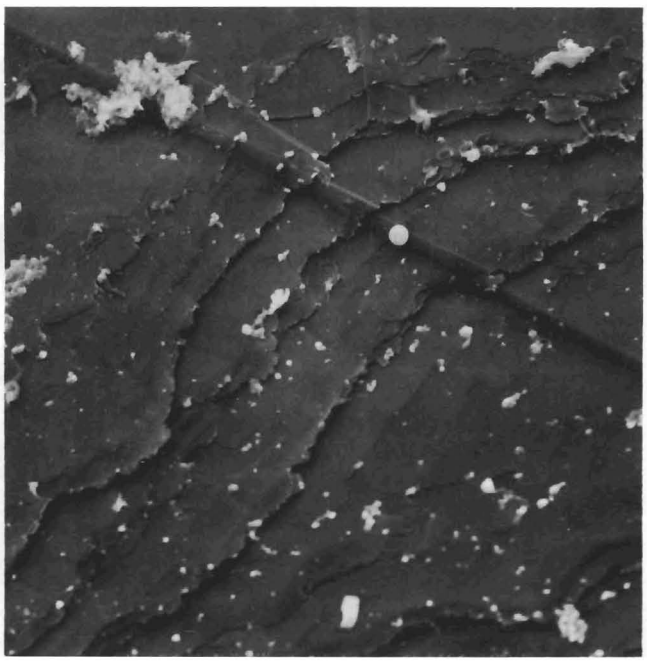

1,600X

4,000X

Uncatalyzed reaction at 1100°C in wet hydrogen causes roughening of edges at ledges and channels.
1100°C; $P_{H_2O}=5\times10^{-2}$ atm. Scanning Electron Micrographs

Figure 11

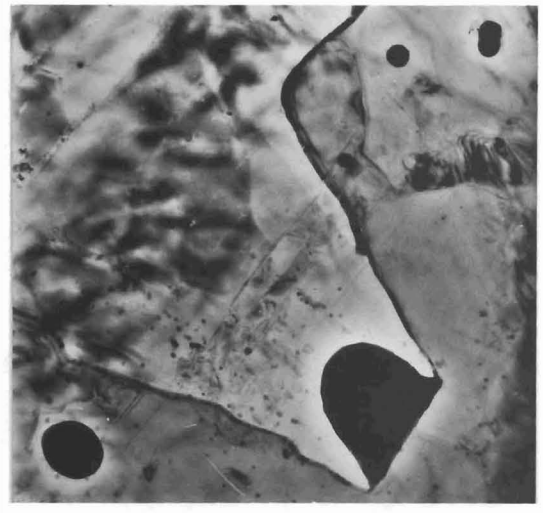

A 15,000X

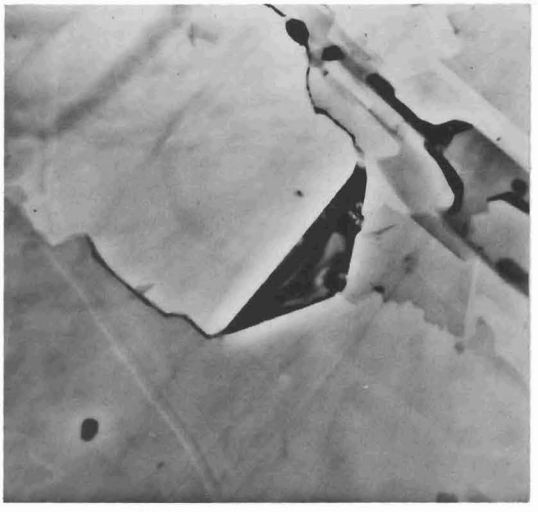

B 15,000X

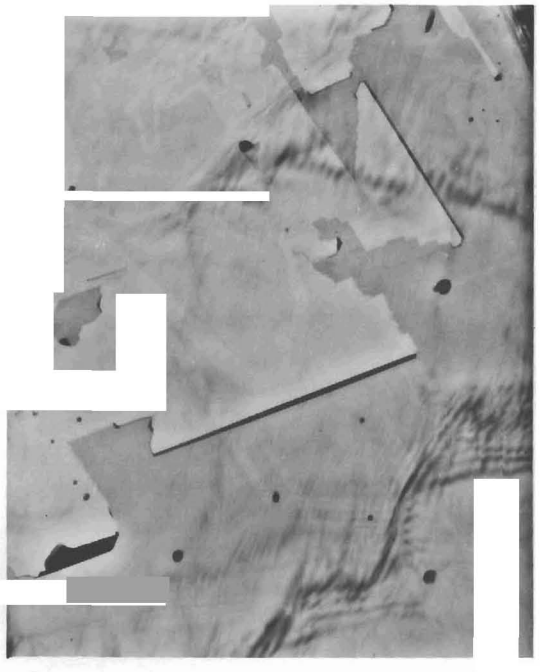

C 10,000X

Examples of reaction channels formed at 1100°C in dry hydrogen. 1100°C; $P_{H_2O}=1.37\times10^{-5}$ atm. Million Volt Electron Micrographs

Figure 12

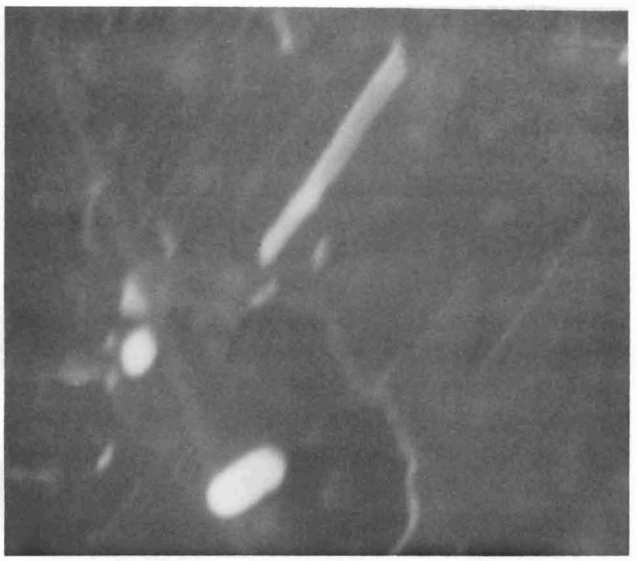

A

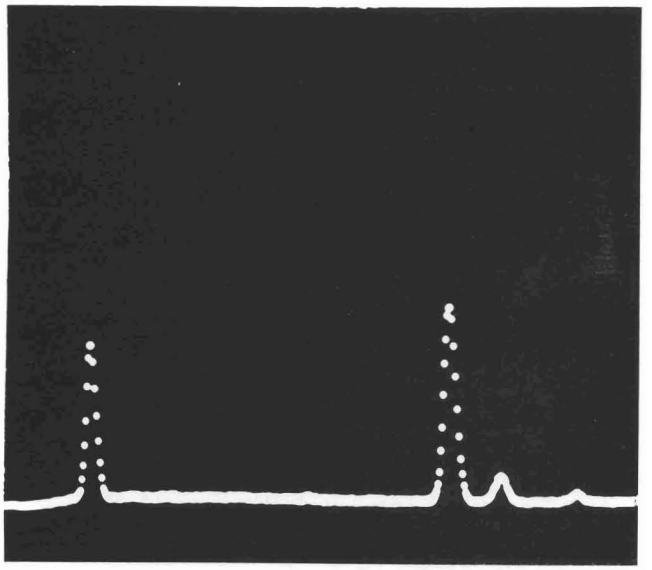

B Si Fe

C Silicon

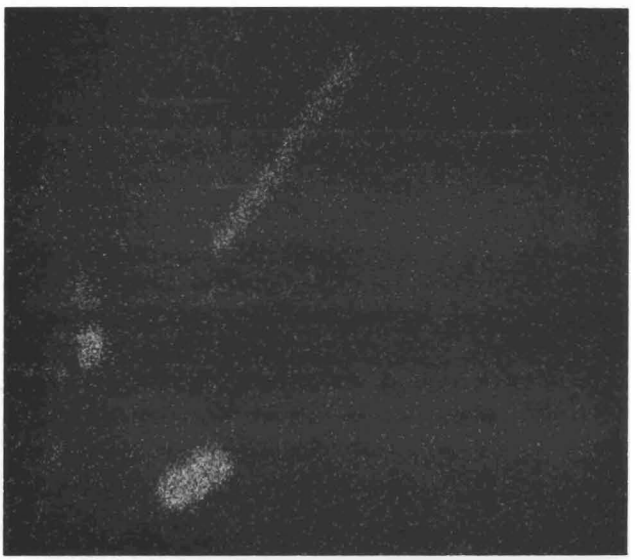

D Iron

X-ray spectra and image maps showing presence of silicon in iron particles after reaction at 1100°C in dry hydrogen. 1100°C; P_{H_2O}=1.37x10^{-5} atm. Scanning Electron Micrographs 8,000X

Figure 13

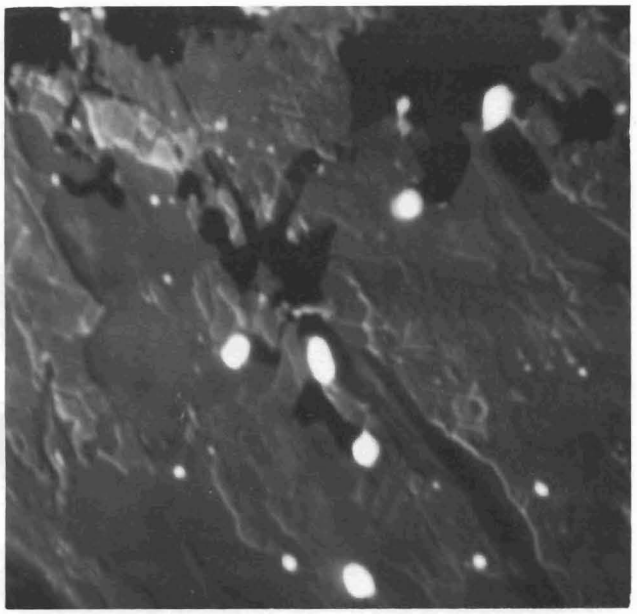

A

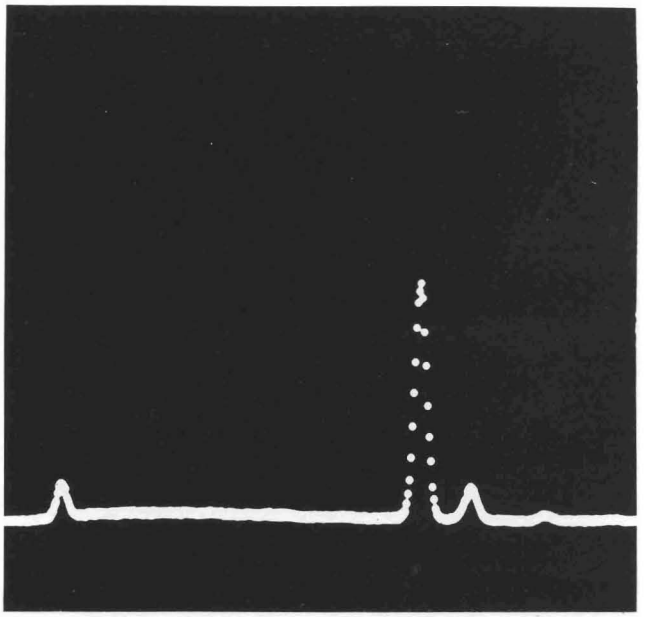

B Si Fe

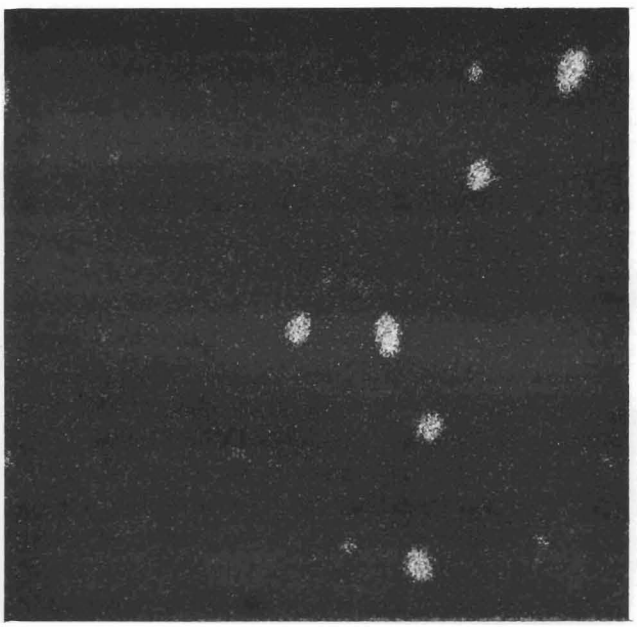

C Iron

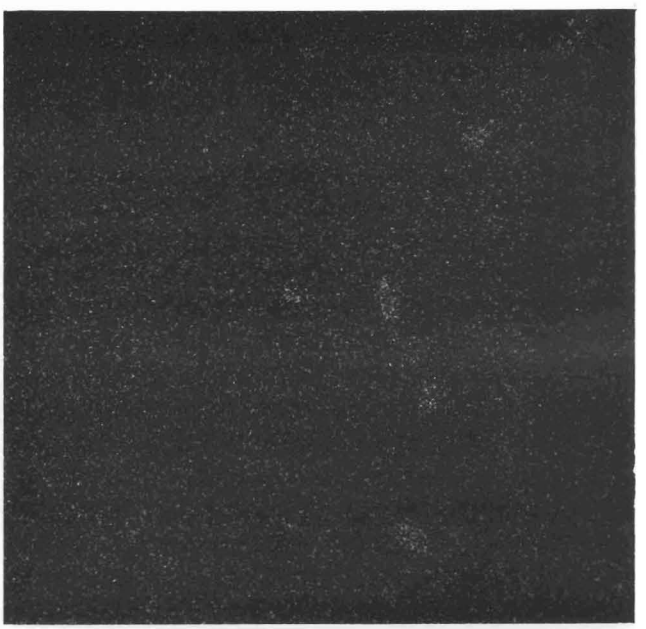

D Silicon

X-ray spectra and image maps showing presence of silicon in iron particles after reaction at 900°C in hydrogen. 900°C; $P_{H_2O}=4x10^{-3}$ atm. Scanning Electron Micrographs 10,000X

Figure 14

Contrast of reaction channels is enhanced by vacuum deposition of gold. 6,000X
1100°C; $P_{H_2O}=4.14\times10^{-4}$ atm. Million Volt Electron Micrograph

Figure 15

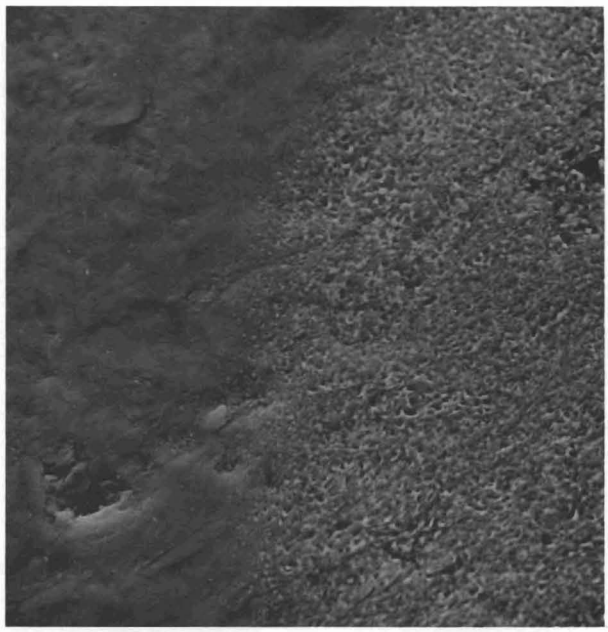

A 800X

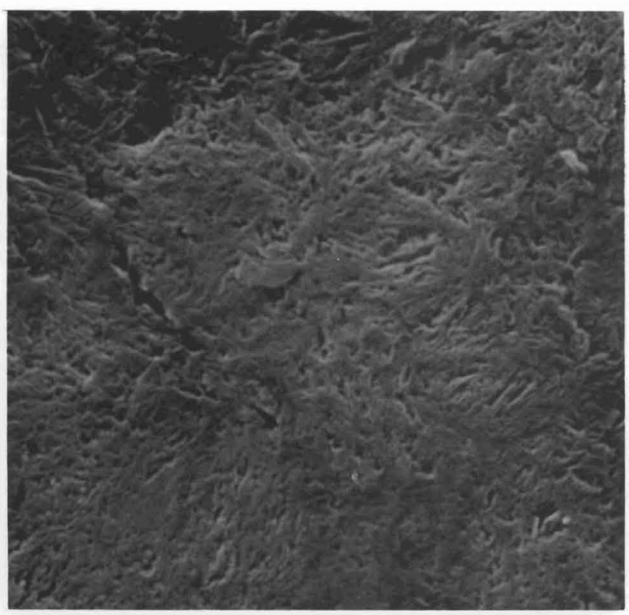

B 16,000X

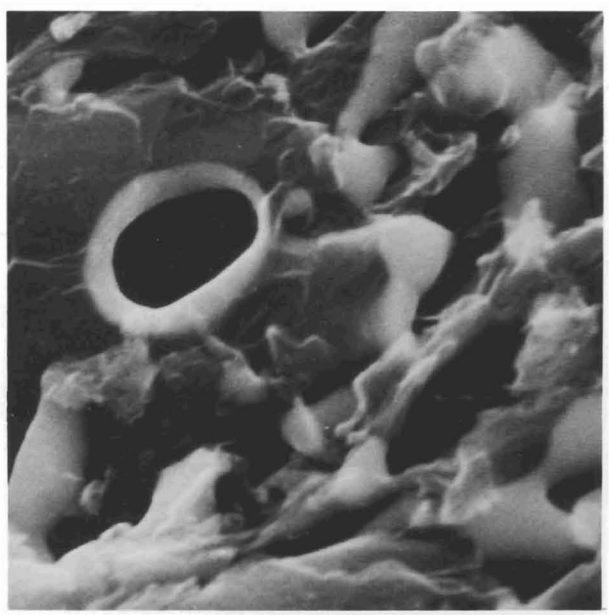

C 16,000X

Gasification of electrode graphite planchet at 1000°C in hydrogen, $P_{H_2O}=1.3\times10^{-5}$ atm.

(A) Boundary between uncoated (left) and iron-coated (right) region. (B) Uncatalyzed reaction zone. (C) Iron catalyzed reaction zone. Scanning Electron Micrographs

Figure 16

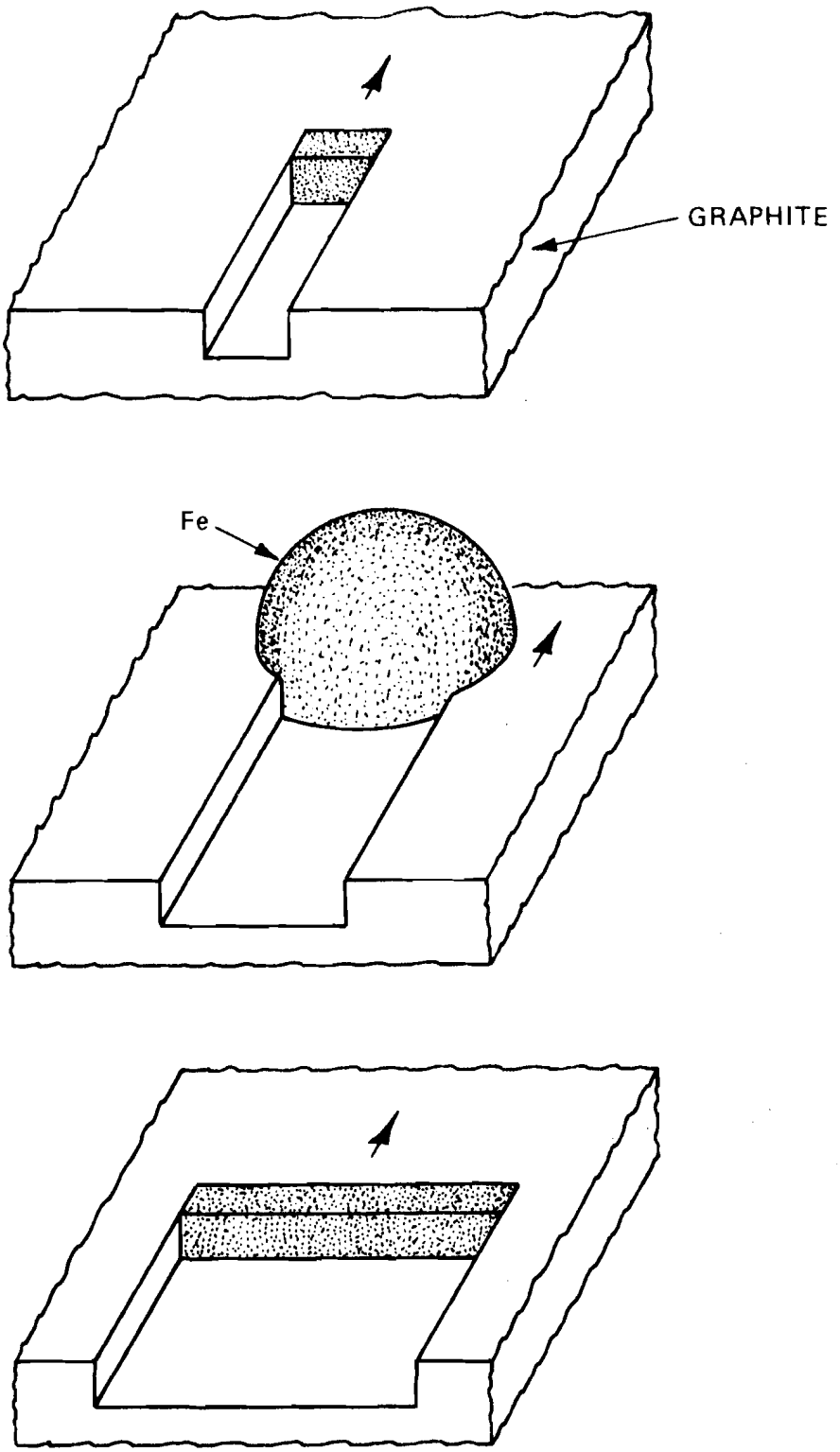

SCHEMATIC ILLUSTRATION OF THREE TYPES
OF REACTION CHANNELS

76-H-025(064)

Figure 17

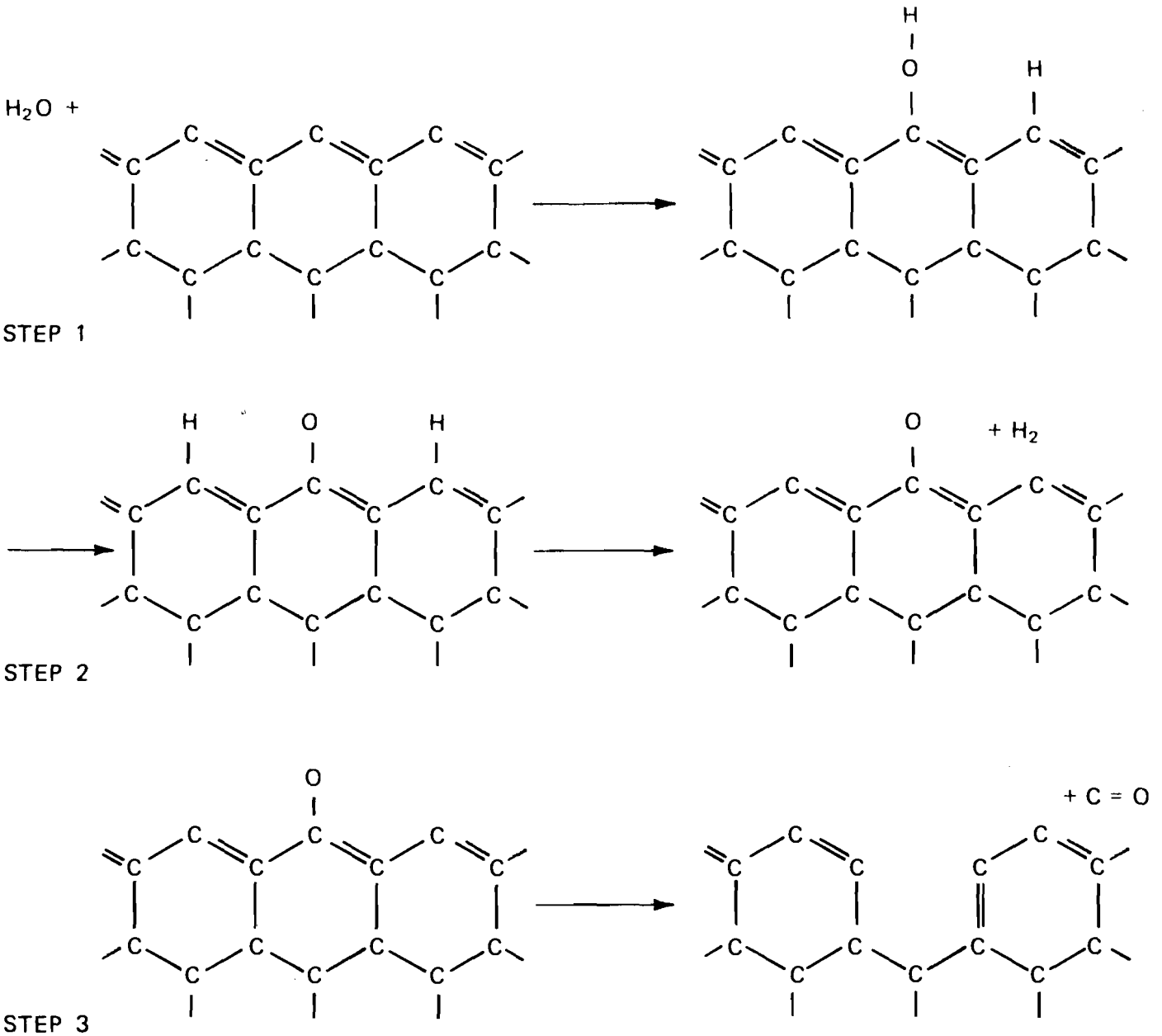

SCHEMATIC ILLUSTRATION OF UNCATALYZED OXIDATION OF EXPOSED BASAL PLANE EDGES OF GRAPHITE

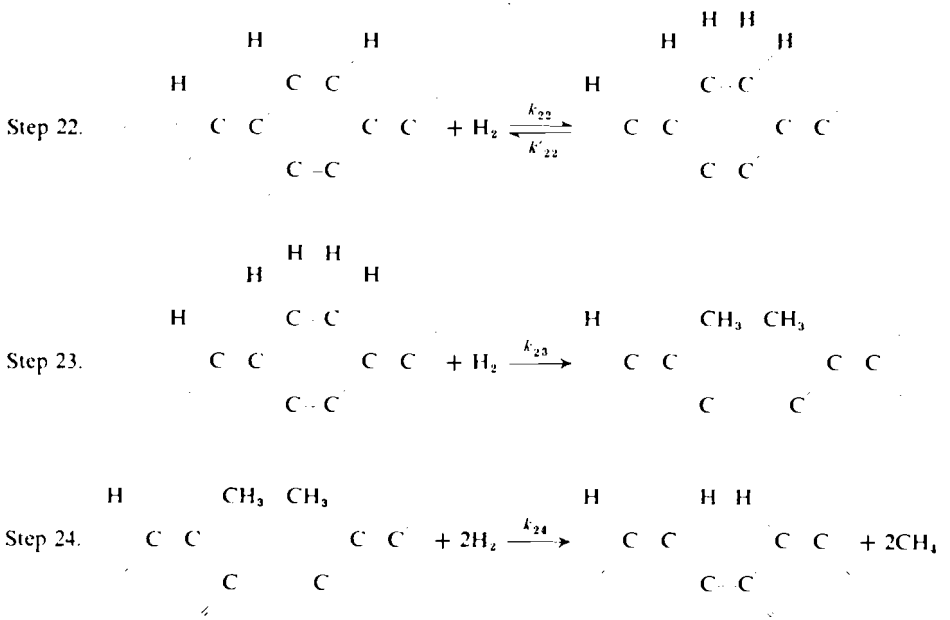

SCHEMATIC ILLUSTRATION OF UNCATALYZED HYDROGENATION OF EXPOSED BASAL PLANE EDGES OF GRAPHITE

76-H-025(064)

Figure 19

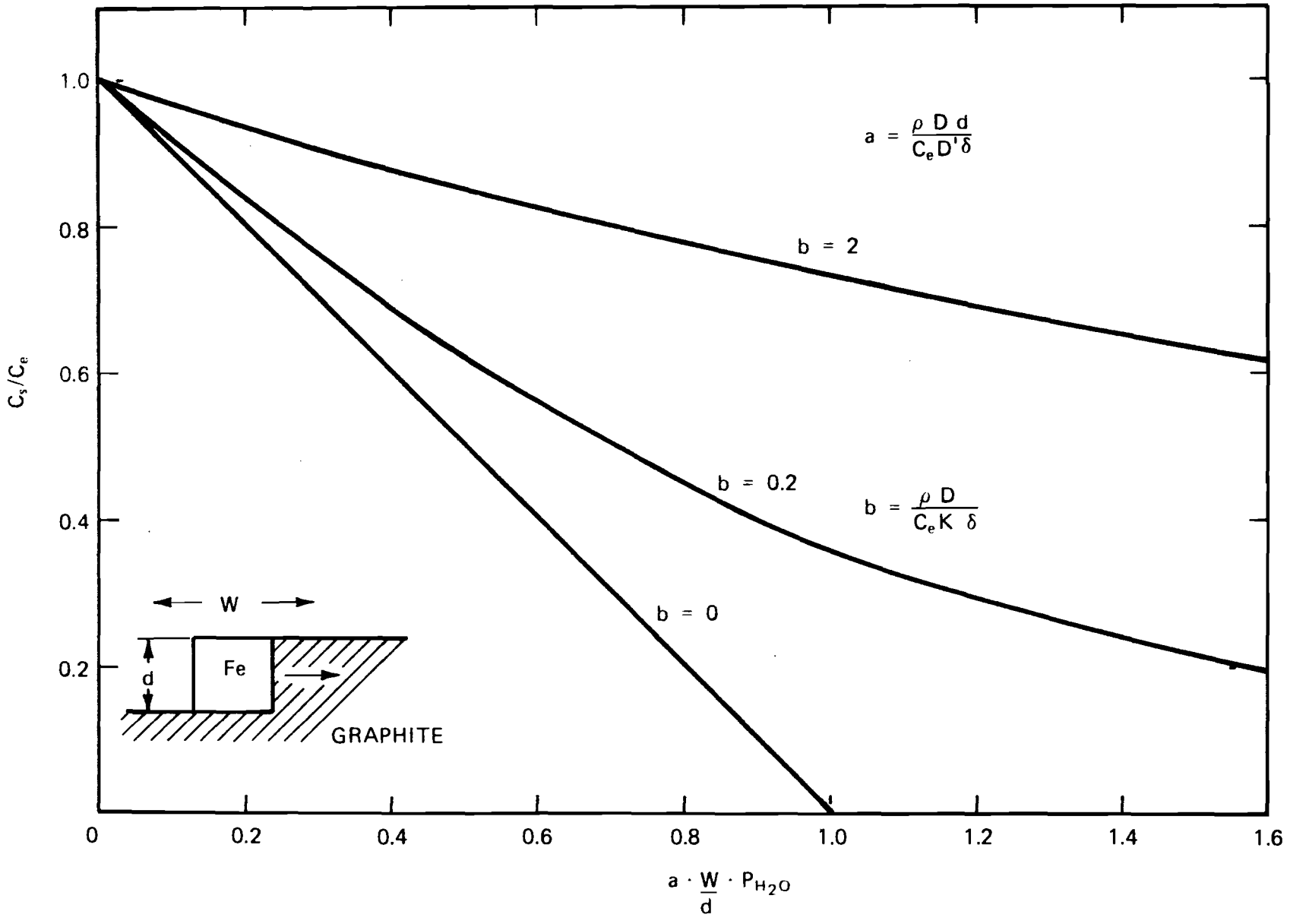

PLOT OF RELATIVE SURFACE CARBON CONCENTRATION ON IRON PARTICLE AS A FUNCTION OF WATER VAPOR PARTIAL PRESSURE AND PARTICLE DIMENSIONS

76-H-025(064)

Figure 20

APPENDIX I

Furnace Control Procedure

Instructions for safe operation of the furnace and gas control system are outlined below. The identification of switches and valves refer to those shown in Figure 1.

ON-OFF PROCEDURE

OFF to RUN

1. TURN ON EXHAUST FAN.
2. OPEN TANK VALVES.
3. TURN ON FURNACE.
4. OPEN VALVES V-3 AND/OR V-4.
5. TURN ON CHART RECORDER.
6. TURN ON S-1 AND WAIT TWO MINUTES.
7. OPEN V-15.
8. SEE "SAMPLE LOADING PROCEDURE."
9. FOLLOW "GAS MIXING PROCEDURE."

RUN to OFF

1. SWITCH OUT GAS FILTER (V-5, V-6) AND SATURATOR (V-10, then V-9).
2. WAIT TWO MINUTES.
3. BYPASS FURNACE TUBE (V-13).
4. CLOSE V-15.
5. TURN S-1 OFF.
6. CLOSE V-3 AND/OR V-4.
7. TURN CHART RECORDER OFF.
8. CLOSE TANK VALVES.
9. TURN EXHAUST FAN OFF.

(LEAVE OXYGEN-SENSOR ON UNLESS SYSTEM WILL NOT BE USED FOR MORE THAN A MONTH.)

SAMPLE UNLOADING AND LOADING PROCEDURES

SAMPLE UNLOADING PROCEDURE

1. IF SYSTEM IS ON "RUN", SWITCH OUT GAS FILTER (V-5, V-6) AND/OR SATURATOR (V-10, THEN V-9).
2. WHEN SAMPLE IS 50°C OR COOLER, BYPASS FURNACE (V-13).
3. GO TO "OFF" IF NOT MAKING ANOTHER RUN IMMEDIATELY; OTHERWISE GO TO STEP 4.
4. REMOVE SAMPLE.
5. GO TO "OFF" OR "LOAD SAMPLE PROCEDURE."

SAMPLE LOADING PROCEDURE

1. ENSURE THAT FURNACE TUBE IS BYPASSED.
2. TURN ON ROUGHING PUMP.
3. PUT SAMPLE BOAT AND BALL BEARING IN TUBE, ATTACH SPRING AND CLAMP.
4. SET V-11, V-12 FOR EVACUATION.
5. AFTER EVACUATION RESET V-11, V-12.
6. CLOSE V-15.
7. PUT FURNACE TUBE IN CIRCUIT (V-13).
8. WAIT TWO MINUTES.
9. OPEN V-15.
10. FOLLOW "GAS MIXING PROCEDURE."
11. SYSTEM IS IN "RUN" STATUS.

GAS MIXING PROCEDURE

1. You are given the desired partial pressure of hydrogen in the final mixture in atm (C) and the desired partial pressure of H_2O in the final mixture (D).

2. Put the furnace tube in-circuit (V-13) and by-pass the filter (F-1) if you want a wet mixture. If you want a dry mixture leave F-1 in the line. Leave the furnace off the quartz furnace tube.

3. Allow purified hydrogen to flow until the oxygen potential stabilizes at some high value (A). The gauge (G-1) should show a slightly positive pressure.

4. Go to the computer, run the program "HYHE" and obtain values E and F. See attached examples.

5. If you want a wet hydrogen mixture (no helium) skip this step and go to the next step. If you do want helium in the mixture, however, adjust the hydrogen and helium flows until the oxygen potential is equal to E (see program). [If the stabilized oxygen potential is greater (less) than E, increase (decrease) the He flow and decrease (increase) the hydrogen flow, keeping the gauge pressure constant at a slightly positive value. Use valves V-1 and V-2. Repeat until the oxygen potential stabilizes to a value as near as practical to E.] Note the actual value of E on the chart.

6. If you want a dry mixture skip this step.
   For a wet mixture do the following (the saturator should be out of the line to start with):
   (a) Open V-8 fully.
   (b) Open V-7 fully.
   (c) Switch in saturator (V-9 first, then V-10).
   (d) Close V-7 until a high bubbling rate is seen.
   (e) Close V-8 until flow just starts to diminish.
   (f) Adjust oxygen potential to equal F (see program) in the following way:
      (1) Coarse: To raise (lower) oxygen potential open (close) V-7 slowly (1 unit on handle/min.).
      (2) Fine: To raise (lower) oxygen potential close (open) V-8 slowly (5 units/min.).

7. This sets the gas mixture. Some minor adjustments of V-8 may be necessary to maintain the oxygen potential E if a wet mixture is used.

```
 RUN

 Wet Helium + Hydrogen Mixture
 HYHE - OXYGEN POTENTIAL FOR DESIRED H20 LEVEL IN HE/H2 MIXTURE

 A - OXYGEN POTL FOR FILTERED HYDROGEN (MILLIVOLTS) ?1450
 B - IMPURITY H20 LEVEL IN FILTERED H2 (AND MIX) IS 1.3768e-05 (AT)
 C - DESIRED PARTIAL PRESS OF H2 IN WET HE+H2 MIX (ATM) ?.6
 D - DESIRED PARTIAL PRESSURE OF H20 IN WET MIX (ATM) ?1.2E-3
 E - SET OXYGEN POTL OF FILTERED HE+H2 MIX TO 1427.5 (MILLIVOLTS)
 F - SET POTL OF WET MIXTURE TO 1230.6 (MILLIVOLTS)

 ready
 *
```

```
          RCM94
password--
[illegible]

SYSTEM ?BASIC
OLD OR NEW-OLD
OLD FILE? /CGS$MOLLY/HYHE
READY
*RUN

 Dry Helium + Hydrogen Mixture (60% Hydrogen)
 HYHE - OXYGEN POTENTIAL FOR DESIRED H2O LEVEL IN HE/H2 MIXTURE

 A - OXYGEN POTL FOR FILTERED HYDROGEN (MILLIVOLTS) ?1450
 B - IMPURITY H2O LEVEL IN FILTERED H2 (AND MIX) IS 1.3768e-05 (AT)
 C - DESIRED PARTIAL PRESS OF H2 IN WET HE+H2 MIX (ATM) ?.6
 D - DESIRED PARTIAL PRESSURE OF H2O IN WET MIX (ATM) ?1.3768E-5
 E - SET OXYGEN POTL OF FILTERED HE+H2 MIX TO 1427.5 (MILLIVOLTS)
 F - SET POTL OF WET MIXTURE TO 1427.5 (MILLIVOLTS)

ready
*RUN

  Wet Hydrogen Mixture (no Helium)
 HYHE - OXYGEN POTENTIAL FOR DESIRED H2O LEVEL IN HE/H2 MIXTURE

 A - OXYGEN POTL FOR FILTERED HYDROGEN (MILLIVOLTS) ?1450
 B - IMPURITY H2O LEVEL IN FILTERED H2 (AND MIX) IS 1.3768e-05 (AT)
 C - DESIRED PARTIAL PRESS OF H2 IN WET HE+H2 MIX (ATM) ?1
 D - DESIRED PARTIAL PRESSURE OF H2O IN WET MIX (ATM) ?1.2E-3
 E - SET OXYGEN POTL OF FILTERED HE+H2 MIX TO 1450.1 (MILLIVOLTS)
 F - SET POTL OF WET MIXTURE TO 1253.1 (MILLIVOLTS)

ready
*
```

same value

APPENDIX II

Gas Composition Analysis Procedure

Instructions for computer calculations of partial pressure of He, H_2, O_2 and H_2O from measured flow rates and oxygen sensor potential are outlined below.

Take strip chart to computer terminal and run "GASCOMP3"

Explanatory notes on questions asked by program:

1. Ambient temperature is the temperature of the flowmeters FM-1 and FM-2.

2. Percent of oxygen in ambient air is usually around 20.6% but can be found by using a standard humidity vs. air composition chart, after the humidity has been noted.

3. Furnace temperature - fairly obvious.

4. Total flow rate is found from the sum of the helium and hydrogen flow rates using the calibration charts.

5. The oxygen potential of the dry helium + hydrogen mixture is the actual value one sets in Step 5 of the "Gas Mixing Procedure."

6. Oxygen potential of purified helium is unimportant except to give an idea of the oxygen impurity level in the cold inlet gases. This number has no effect on the gas composition tabulated by the computer. (Choose 285 mV if in doubt.)

7. Oxygen potential of purified hydrogen is obtained in Step 3 of the "Gas Mixing Procedure."

8. The oxygen potential of the wet gas is obtained in Step 6 of the "Gas Mixing Procedure."

```
 OLD
OLD FILE? /CGS$MOLLY/GASCOMP3
READY
*RUN


GASCOMP3 - COMPOSITIONS OF GASES IN FURNACE 04/28/77

.AMBIENT TEMPERATURE (DEG C)  ?22

 PERCENT OF O2 IN AMBIENT AIR ?20.6

 FURNACE TEMPERATURE (DEG C)  ?850

 TOTAL FLOW RATE (ML/MIN)     ?1000

 OXYGEN POTL OF DRY H2+HE MIX ?1429

 WHAT IS THE OXYGEN POTENTIAL OF
 (1) PURIFIED HELIUM   (MV)   ?285
 (2) PURIFIED HYDROGEN (MV)   ?1450

 THE OXYGEN AND WATER IMPURITY LEVELS ARE AS FOLLOWS
OXYGEN (PPM)     .50
WATER  (PPM)   12.77

 WHAT IS THE POTENTIAL FOR THE WET GAS ?1232

 WATER VAPOR PRESSURE IN SATURATOR IS    .9 MM HG

 FLOWS AND PRESSURES FOR GASES IN FURNACE AT  850.0 (DEG C)
      GAS       FLOW RATE (ML/MIN)    PARTIAL PRESSURE (ATM)
    HELIUM          1.443e 03              3.785e-01
  HYDROGEN          2.364e 03              6.202e-01
    OXYGEN          7.506e-20              1.969e-23
    WATER           4.576e 00              1.201e-03
    TOTAL           3.811e 03              1.000e 00

 R*T*LN(P02) (= DELTA F) IS  -116.7 (KILOCALORIES)
```

OXYGEN SENSOR CALIBRATION

1. Start from standby.
2. Open V-4.
3. Set flow to 100 on FM-1.
4. Turn on S-1.
5. Open V-15.
6. Wait until cell potential falls to less than 1000 mV.
7. Close V-15.
8. Close V-4.
9. Close V-16.
10. Open V-17.
11. Open V-15.
12. Set V-19 so that FM-3 reads 3.5.
13. Wait until cell potential stabilizes.
14. Adjust S-5 until cell potential reads zero.
15. Close V-15.
16. Close V-17
17. Open V-16 (to l.h. port).
18. Open V-4.
19. Wait two minutes.
20. Open V-15.
21. Wait until cell potential reaches 200 mV.
22. Close V-15.
23. Close V-4.
24. System is on standby.

List for "HYHE"

```
LIST

1000 PRINT USING 1020,
1010 PRINT\PRINT
1020 "HYHE - OXYGEN POTENTIAL FOR DESIRED H2O LEVEL IN HE/H2 MIXTURE
1030 PRINT "A - OXYGEN POTL FOR FILTERED HYDROGEN (MILLIVOLTS) ";
1040 INPUT E1
1050 A=10^(9.425617-E1/101.49276)
1060 PRINT\PRINT USING 1070,A\PRINT
1070"B - IMPURITY H2O LEVEL IN FILTERED H2 (AND MIX) IS #.####^^^^ (AT)
1080 PRINT "C - DESIRED PARTIAL PRESS OF H2 IN WET HE+H2 MIX (ATM) ";
1090 INPUT X
1100 PRINT
1110 PRINT "D - DESIRED PARTIAL PRESSURE OF H2O IN WET MIX (ATM) ";
1120 INPUT B
1130 X=X/(1-B)
1140 E2=101.49276*(CLG(X)-CLG(A)+9.425617)
1150 PRINT
1160 PRINT USING 1170,E2
1170"E - SET OXYGEN POTL OF FILTERED HE+H2 MIX TO ####.# (MILLIVOLTS)
1180 E3=101.49276*(CLG(X*(1-B))-CLG(B)+9.425617)
1190 PRINT\PRINT USING 1200,E3\PRINT
1200"F - SET POTL OF WET MIXTURE TO ####.# (MILLIVOLTS)
1210 STOP
1220 END

ready
```

*

List for "GASCOMP3"

```
1000 PRINT "GASCOMP3 - COMPOSITIONS OF GASES IN FURNACE ";DAT$
1010 DIM U9(2)
1020 DEF FNA(X7)
1030 A7=12499/(273+X7)-.69477*CLG(273+X7)-6.20303E-4*(273+X7)
1040 C7=3.25395E-7*(273+X7)^2-5.98675E-11*(273+X7)^3
1050 FNA=A7+C7
1060 FNEND
1070 PRINT\PRINT\PRINT "AMBIENT TEMPERATURE (DEG C)  ";
1080 INPUT T1
1090 T2=T1
1100 PRINT\PRINT "PERCENT OF 02 IN AMBIENT AIR ";
1110 INPUT B7
1120 PRINT\PRINT "FURNACE TEMPERATURE (DEG C)  ";
1130 INPUT T3
1140 PRINT\PRINT "TOTAL FLOW RATE (ML/MIN)     ";
1150 INPUT Z4
1160 PRINT\PRINT "OXYGEN POTL OF DRY H2+HE MIX ";
1170 INPUT Z5
1180 PRINT\PRINT "WHAT IS THE OXYGEN POTENTIAL OF "
1190 PRINT "(1) PURIFIED HELIUM   (MV)   ";\INPUT V1
1200 PRINT "(2) PURIFIED HYDROGEN (MV)   ";\INPUT V2
1210 I1=1E6*10^(CLG(B7/100)-V1/50.74638)
1220 I2=1E6*10^(9.768682+.5*CLG(B7/100)-V2/101.49276)-2*I1
1230 I8=(2*I1+I2)*1E-6
1240 I7=10^(CLG(I8)-9.768682-.5*CLG(B7/100)+Z5/101.49276)
1250 A=Z4*I7*.0121875/(273+T1)
1260 B=Z4*(1-I7)*.0121875/(273+T1)
1270 PRINT\PRINT "THE OXYGEN AND WATER IMPURITY LEVELS ARE AS FOLLOWS"
1280 PRINT USING 1290,I1
1290:OXYGEN (PPM) ###.##
1300 PRINT USING 1310,I2
1310:WATER  (PPM) ###.##
1320 PRINT\PRINT "WHAT IS THE POTENTIAL FOR THE WET GAS ";
1330 INPUT R9
1340 R=10^(.5*CLG(B7/100)-.0098529*R9+9.768682+CLG(I7))
1350 P=R/(1+R)
1360 K2=FNA(T3)
1370 P2=760*P
1380 PRINT
1390 PRINT USING 1400,P2
1400:WATER VAPOR PRESSURE IN SATURATOR IS ###.# MM HG
1410 Q9=25
1420 IF P2<4.6 THEN 1480
1430 IF P2>3577 THEN 1480
1440 Q9=24
1450 GOSUB 1820
1460 PRINT USING 1470,T2
```

LIST FOR "GASCOMP3" (cont'd.)

```
1470:(EFFECTIVE SATURATOR TEMPERATURE IS ####.# DEG C)
1480 REM
1490:      GAS        FLOW RATE (ML/MIN)     PARTIAL PRESSURE (ATM)
1500:    HELIUM           #.###^^^^               #.###^^^^
1510:  HYDROGEN           #.###^^^^               #.###^^^^
1520:    OXYGEN           #.###^^^^               #.###^^^^
1530:    WATER            #.###^^^^               #.###^^^^
1540:    TOTAL            #.###^^^^               #.###^^^^
1550 Q3=2*(CLG(P)-K2-CLG(I7*(1-P)))
1560 X3=10^Q3
1570 J5=(1-P)*(1-I7)
1580 Y3=(1-P)*I7
1590 Z3=P
1600 W3=1.
1610 W2=82.051282*(273+T3)*(A+B)/(1-P)
1620 J4=J5*W2
1630 Y2=Y3*W2
1640 X2=X3*W2
1650 Z2=Z3*W2
1660 PRINT
1670 PRINT USING 1680,T3
1680:FLOWS AND PRESSURES FOR GASES IN FURNACE AT ####.# (DEG C)
1690 PRINT USING 1490,
1700 PRINT USING 1500,J4,J5
1710 PRINT USING 1510,Y2,Y3
1720 PRINT USING 1520,X2,X3
1730 PRINT USING 1530,Z2,Z3
1740 PRINT USING 1540,W2,W3
1750 B6=4.575*(T3+273)*CLG(X3)/1000
1760 PRINT\PRINT USING 1770,B6
1770:R*T*LN(P02) (= DELTA F) IS #####.# (KILOCALORIES)
1780 FOR K= 1 TO 09
1790 PRINT
1800 NEXT K
1810 STOP
1820 IF P2>149.4 THEN 1850
1830 T2=1750.286/(8.10765-CLG(P2))-235
1840 RETURN
1850 T2=1668.21/(7.96681-CLG(P2))-228
1860 RETURN
1870 END

ready

*


 BYE
*resources   3.68 to date:       19.86=  0%
**on at 14.346 - off at 14.625 on  04/28/77
```

APPENDIX III

Calculation of Equilibrium Gas Composition

Calculations of thermodynamic equilibrium for complex gas-solid systems can be obtained with a utility computer program (see abstract below) which employs a free-energy minimization alogrithm. With this program, the formation or reaction of specific chemical species can be suppressed, thereby enabling conditions at partial equilibrium to be examined computationally. Results of some calculations for C(s) - H_2O - H_2 - CH_4 - CO - CO_2 - O_2 systems are shown in Figures III-A and III-B.

Thermodynamic Equilibrium by Free-Energy Minimization:
Ideal Solutions

F. C. Schwerer
U. S. Steel Corporation Research Laboratory
Monroeville, Pennsylvania 15146

Abstract

The solutions of some problems concerned with the reaction of solid or liquid materials with a gaseous environment at elevated temperatures proceed more efficiently with knowledge of the type and concentration of chemical species that would be present under specified conditions of complete or partial thermodynamic equilibrium. From basic thermodynamic principles, chemical equilibrium in a reacting system is determined by the condition that the free energy be minimum subject to certain external constraints.

A FORTRAN subroutine has been developed to calculate the concentration of chemical species present at constant temperature and pressure in a general system containing fixed-composition condensed phases, ideal condensed solutions, and an ideal gas mixture by minimizing the total free energy subject to the constraint that the number of atom-weights of each element be conserved. For convenient utilization of this computational procedure in an interactive mode from a teletype terminal, this subroutine has been incorporated with a special input-output program and with a library of thermodynamic data for some common steel-related chemical species.

This report contains operational information for easy use of this computational package along with a brief description of (1) the algorithm for the minimization of the free energy and (2) the format of the input-output program and the data library.

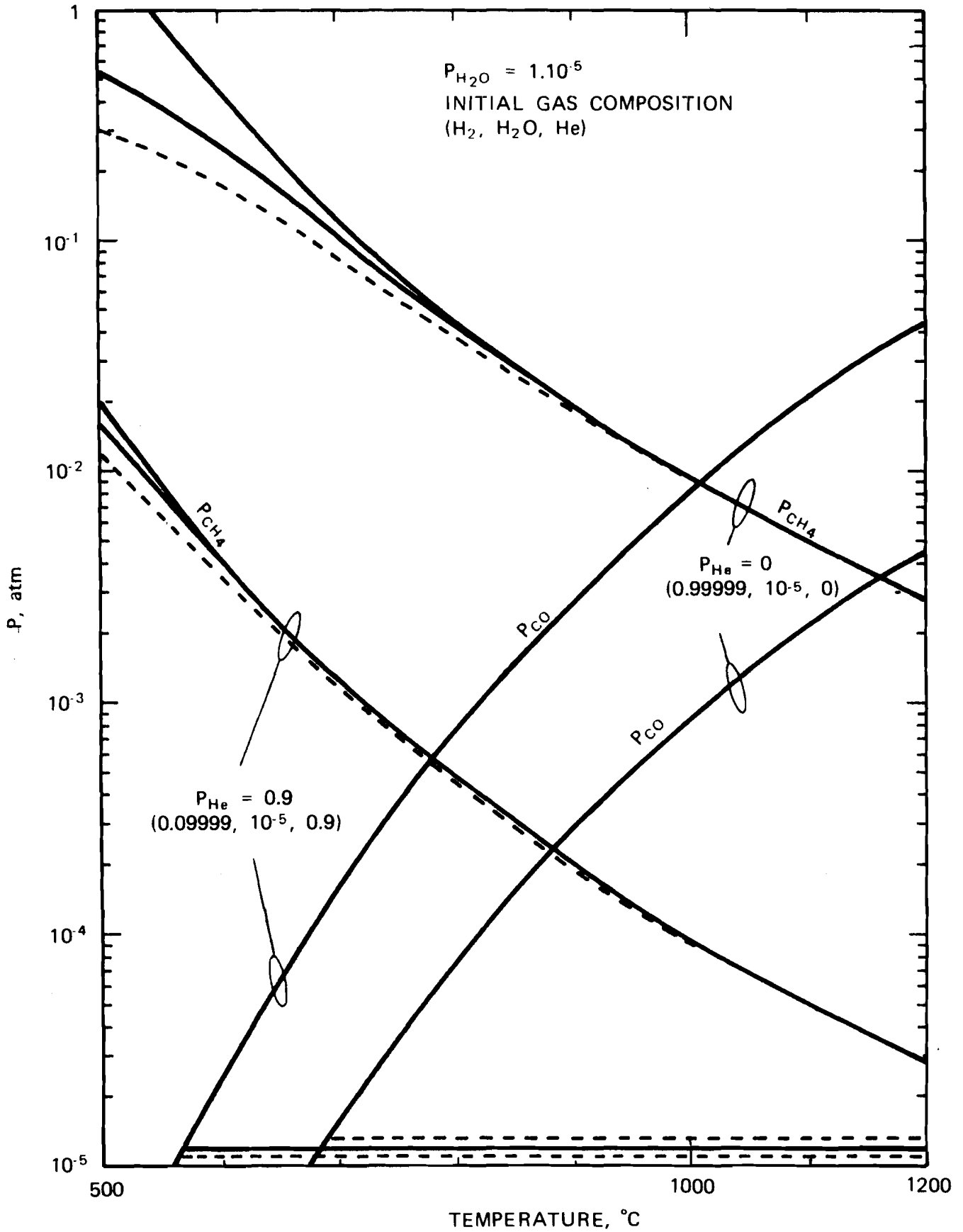

EQUILIBRIUM PRESSURES OF CO AND CH_4 CALCULATED (1) FOR H_2-C(s) OR H_2O-C(s) REACTIONS ASSUMING INLET GAS COMPOSITIONS MAINTAINED AT REACTION SURFACE (SOLID CURVES) AND LOCAL REACTION EQUILIBRIUM (DASHED CURVES) AND (2) FOR FULL EQUILIBRIUM IN C-CO-CO_2-CH_4-O_2 SYSTEM. INLET GAS COMPOSITION: 10^{-5} ATM H_2O, 0 AND 0.9 ATM He, BALANCE H_2.

76-H-025(064)

Figure A-1

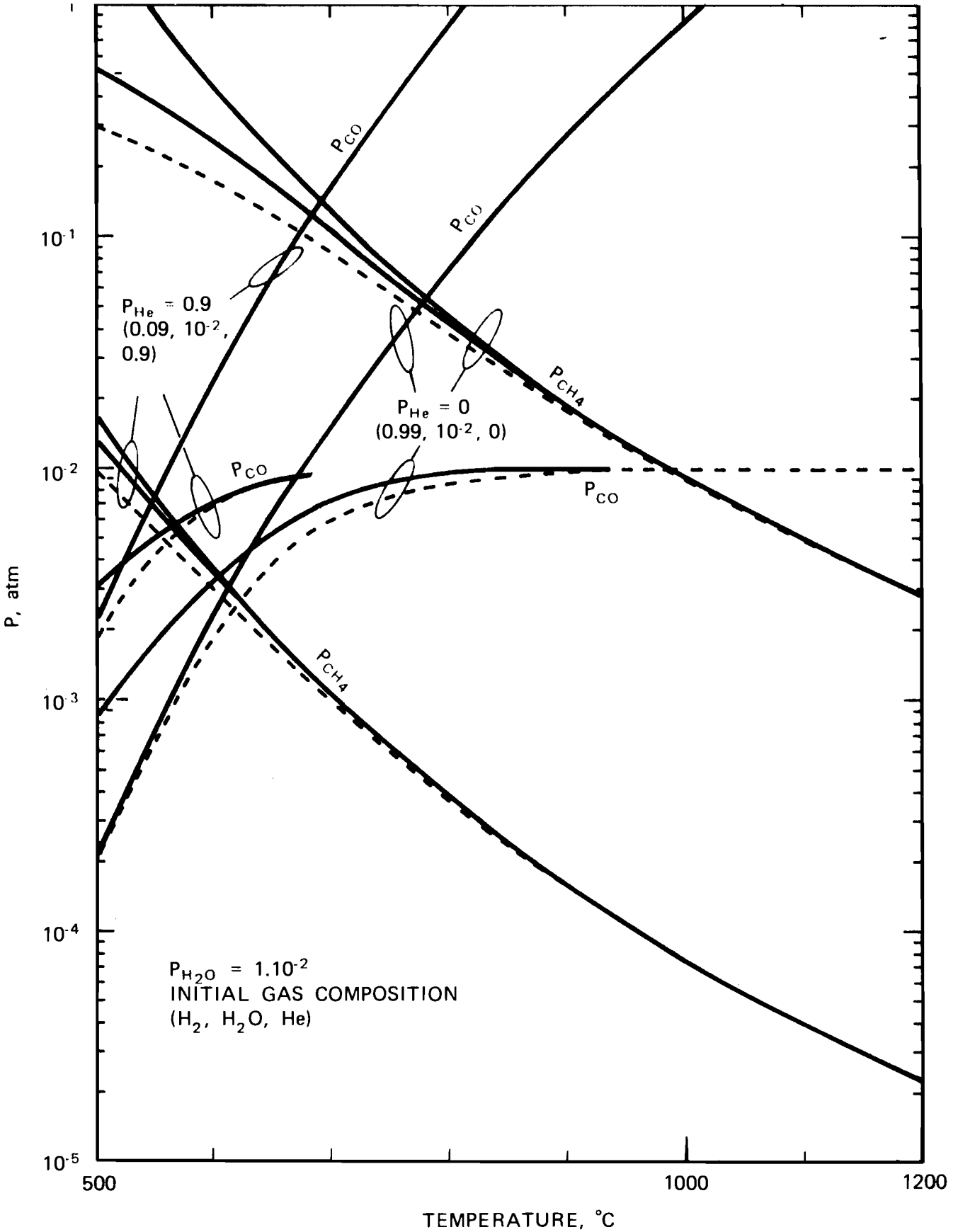

EQUILIBRIUM PRESSURES OF CO AND CH_4 CALCULATED (1) FOR H_2-C(s) OR H_2O-C(s) REACTIONS ASSUMING INLET GAS COMPOSITIONS MAINTAINED AT REACTION SURFACE (SOLID CURVES) AND LOCAL REACTION EQUILIBRIUM (DASHED CURVES) AND (2) FOR FULL EQUILIBRIUM IN C-CO-CO_2-CH_4-O_2 SYSTEM. INLET GAS COMPOSITION: 10^{-2} ATM H_2O, 0 AND 0.9 ATM He, BALANCE H_2.

76-H-025(064)

Figure A-2

APPENDIX IV

Institute On Scientific Problems Relevant To Coal Utilization

WEST VIRGINIA UNIVERSITY **MAY 23-25, 1977**

Abstract

ELECTRON MICROSCOPE STUDIES OF IRON-CATALYZED GASIFICATION OF GRAPHITE

R.M. Fisher, C.G. Shirley, A. Szirmae and J.V. Mahoney
U.S. Steel Research Laboratory, Monroeville, Pa. 15146

The pronounced catalytic effect of iron on the reaction of carbonaceous solids with various gases (O_2, CO-CO_2, H_2O-H_2) has been documented by a number of investigators reporting on thermogravimetric studies on bulk samples and on optical and electron microscope observations of pitting or surface channeling by rapid local attack adjacent to sub-micron iron particles. In this work, emphasis has been placed on detailed electron microscope studies of Fe particle channeling on graphite exposed to "wet" and "dry" hydrogen (P_{H_2O} 3×10^{-2} $\sim6\times10^{-6}$) at temperatures from 650°C to 1200°C. The scanning and million volt transmission electron micrographs to be displayed at the poster session illustrate the wide variation in channel appearance which occurs depending on temperature and/or P_{H_2O}. The straight narrow channels typical of oxidation reactions are less evident as the temperature is raised and the water content decreased. Instead, wavy channels result from the "tracks" of large spherical particles moving over the surface. At the highest temperatures and/or driest atmosphere the iron wets the graphite and spreads out as a thin film along the edge of extremely broad terraces. Speculative models of the reactions responsible for channel characteristics will also be illustrated. This research is supported by the ERDA Div. of Physical Research contract No. E (11-1)-2933.

APPENDIX V

Annual Meeting Electron Microscopy Society of America, Boston, Mass. August 22-26, 1977.

Abstract

ELECTRON OPTICAL STUDIES OF CATALYZED GASIFICATION OF GRAPHITE

A. Szirmae, C. G. Shirley and R. M. Fisher

U.S. Steel Corp., Research Laboratory, Monroeville, Pa. 15146

The pronounced catalytic effect of small particles of iron and other elements and compounds on the reaction of carbonaceous solids with various gases (O_2, $CO-CO_2$, H_2O-H_2) has been documented by a number of investigators reporting on thermogravimetric studies on bulk samples (1,2) and on optical and electron microscope observations of pitting or surface channeling by rapid local attack adjacent to sub-micron iron particles (3,4). In this work, emphasis has been placed on detailed electron microscope studies of Fe particle channeling on graphite exposed to "wet" and "dry" hydrogen (P_{H_2O} 3×10^{-2} $\sim6\times10^{-6}$) at temperatures from 650°C to 1200°C.

Flakes of freshly cleaved Ticonderoga graphite are coated with 40 - 1000 Å of Fe by vacuum deposition which forms spherical particles during subsequent annealing at 750°C. Specimens are reacted for from 5-90 minutes in H_2-H_2O-He atmospheres and examined in the USS-MVEM or an ETEC-SEM. SEM and MVEM observations of the surface channels resulting from the Fe-catalyzed reaction producing CO and/or CH_4 have revealed variations in their nature which are dependent upon temperature and P_{H_2O} level. Very narrow, parallel-sided channels, initiated at ledge steps on the cleaved graphite, take on $<11\bar{2}0>$ directions at lower temperatures, whereas at higher temperatures broad wavy tracks are left by iron particles which continue to grow by the addition of other iron particles encountered in their path.

At 1100°C in very dry hydrogen, the edges of the very broad reaction zones are wetted by the iron phase forming thin single crystal ribbons. The electron diffraction patterns of these particles have not been identified. Spectrochemical analysis in the SEM of specimens reacted above 900°C has revealed the presence of a large amount of Si in the particles which may originate from impurities in the graphite or possibly from the quartz furnace tube. Measurements of the length of the longest channels on selected specimens show a variation of not more than a factor of 20 over the full temperature range in keeping with a low (~10 kcal) activation energy.

This research is supported by ERDA, Division of Physical Research, Contract No. E(11-1)-2933.

1. H.H. Lowry, ed., Chemistry of Coal Utilizztion, Suppl. Vol., (John Wiley and Sons, Inc., New York, 1963).
2. E.T. Turkdogan and J.V. Vinters, Carbon 10, 97 (1972).
3. R.T.K. Baker and P.S. Harris, Carbon 11, 25 (1973).
4. D.W. McKee, Carbon 12, 453 (1974).

Fig. 1 - Fe-catalyzed reaction zones.

(A) SEM - 16,000X; 850°C - $P_{H_2O} = 2 \times 10^{-2}$ atm.

(B) MVEM - 5,000X; 1100°C - $P_{H_2O} = 4 \times 10^{-4}$ atm.

(C) MVEM - 22,500X; 1100°C - $P_{H_2O} = 10^{-5}$ atm.

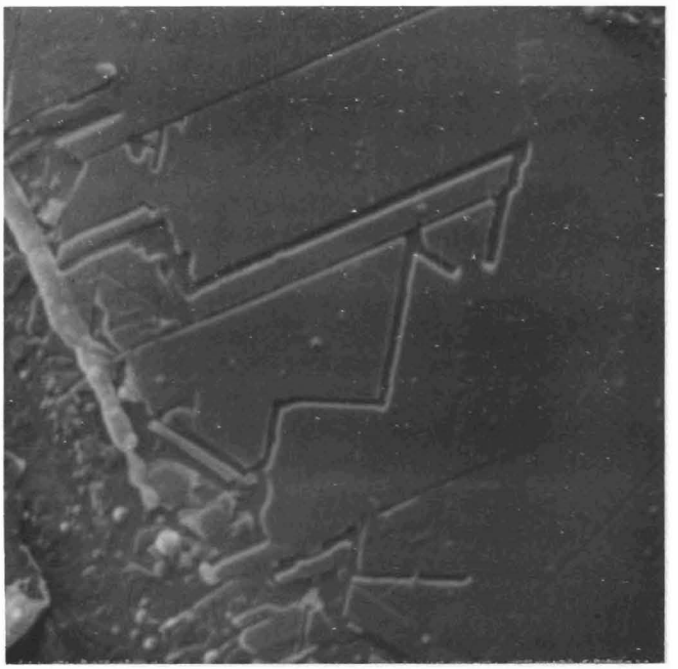

(A)

(B)

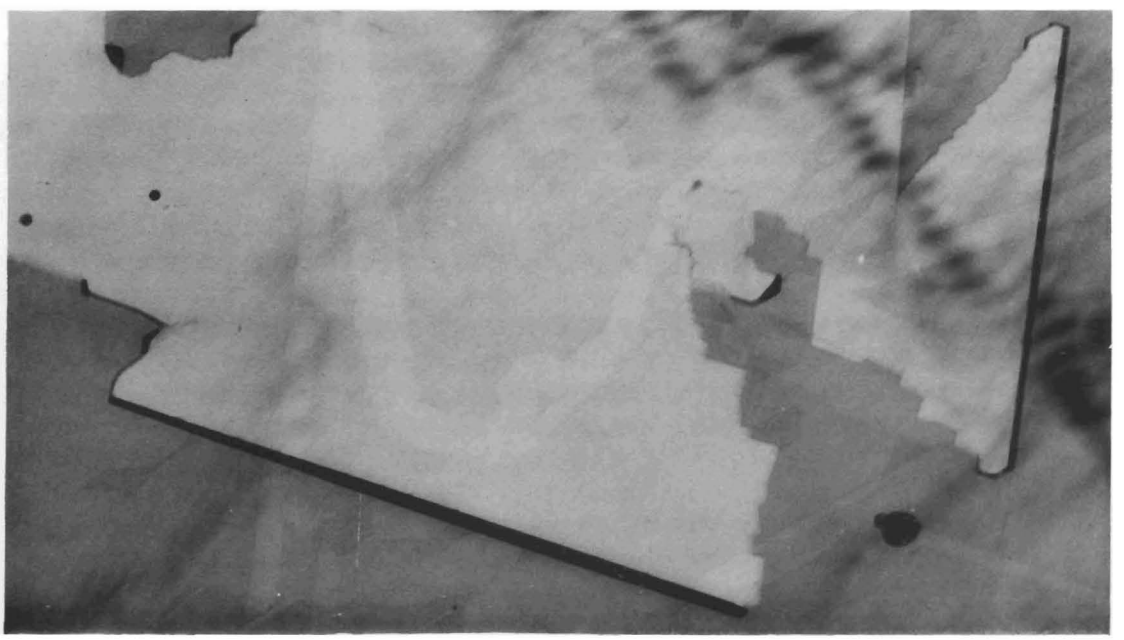

(C)